A MULTI-FACETED STUDY OF NEMATIC ORDER RECONSTRUCTION IN MICROFLUIDIC CHANNELS.*

JAMES DALBY†, YUCEN HAN†, APALA MAJUMDAR*†, AND LIDIA MRAD‡

Abstract. We study order reconstruction (OR) solutions in the Beris-Edwards framework for nematodynamics, for both passive and active nematic flows in a microfluidic channel. OR solutions exhibit polydomains and domain walls, and as such, are of physical interest. We show that OR solutions exist for passive flows with constant velocity and pressure, but only for specific boundary conditions. We prove the existence of unique, symmetric and non-singular nematic profiles, for boundary conditions that do not allow for OR solutions. We compute asymptotic expansions for OR-type solutions for passive flows with non-constant velocity and pressure, and active flows, which shed light into the internal structure of domain walls. The asymptotics are complemented by extensive numerical studies that demonstrate the universality of OR-type structures in static and dynamic scenarios.

Key words. Nematodynamics, Active liquid crystals, Microfluidics

AMS subject classifications. 34A20, 34E10, 76A15

1. Introduction. Nematic liquid crystals (NLCs) are mesophases that combine fluidity with the directionality of solids [14]. The molecules of NLCs tend to align along certain locally preferred directions, leading to a degree of long-range orientational order. This partial ordering results in direction-dependent physical properties that render them suitable for a range of industrial applications, including their widespread use in optical displays. When confined to thin planar cells or channels and in the presence of fluid flow, applications of nematics are further extended, for example, to optofluidic devices and guided micro-cargo transport through microfluidic networks [12, 31]. These hydrodynamic applications are facilitated by the intrinsic coupling between the fluidity and the NLC orientational ordering, leading to unusual and exceptional mechanical and rheological properties [28].

Flow-induced deformation of nematic textures in confinement are ubiquitous, both in passive systems where the hydrodynamics are driven by external agents, and also in active systems. Active matter systems, composed of self-driven units, also exhibit orientational ordering and collective motion, resulting in a wealth of intriguing non-equilibrium properties [27]. We focus on passive and active nematodynamics in microfluidic channels, with a view to model and analyse spatio-temporal pattern formation and the stability of singular lines or domain walls in such channels.

We work with long, shallow three-dimensional microfluidic channels of width L, in a reduced Beris-Edwards framework [4]. Our domain is effectively one-dimensional, since we assume that structural details are invariant across the length and height of the channel, and we work with a reduced Landau-de Gennes $\mathbf{Q}$-tensor for the nematic ordering. This reduced $\mathbf{Q}$-tensor incorporates information about the nematic director, $\mathbf{n}$, and the degree of nematic ordering. The director $\mathbf{n}$ is parameterised by an angle,

*Submitted to the editors DATE.

Funding: AM is supported by the University of Strathclyde New Professors Fund, a Leverhulme International Academic Fellowship, an OCIAM Visiting Fellowship at the University of Oxford and a Daiwa Foundation Small Grant. JD acknowledges support from the University of Strathclyde and the DST-UKIERI. YH is supported by a Royal Society Newton International Fellowship.

†Department of Mathematics, University of Strathclyde, UK (james.dalby@strath.ac.uk, apala.majumdar@strath.ac.uk, yucen.han@strath.ac.uk).

‡Department of Mathematics and Statistics, Mount Holyoke College, Massachusetts, USA (lmrad@mtholyoke.edu).

θ, which describes the in-plane alignment of the nematic molecules, and a scalar order parameter, s, which measures the degree of orientational order about the director $\mathbf{n}$. We consider steady unidirectional flows, which, within the Beris-Edwards framework, result in a system of non-linear, coupled differential equations for s, θ, and the fluid velocity $\mathbf{u}$. There are three dimensionless variables, two of which are related to the nematic fluidity, and the third dimensionless parameter, L^*, is inversely proportional to L^2 and plays a key role in the stability of singular structures.

Our work is largely devoted to *Order Reconstruction* (OR) solutions (defined precisely in section 3). OR solutions are nematic profiles with distinct director polydomains, separated by singular lines or singular surfaces, referred to as domain walls. OR solutions are relevant for modelling chevron or zigzag patterns observed in pressure-driven flows [1, 11], as well as in active nematics where aligned fibers confined in narrow channels can be controlled to display a laminar flow [20]. OR solutions have been studied in purely nematic systems, for example [23], [9] and [8]. Additionally, OR solutions are not limited to purely nematic systems e.g. OR solutions exist in ferronematic systems comprising magnetic nanoparticles in NLC media [13]. Generalized OR solutions or OR-type solutions/instabilities (defined in section 4) are also observed in smectics and cholesterics. For example, when a cell filled with a smectic-A liquid crystal is cooled to the smectic-C phase, a similar chevron texture is observed and has been the impetus of considerable experimental and theoretical interest [30, 25, 29].

We thus speculate that OR solutions are a universal property of partially ordered systems, specifically systems with free energies that employ a Dirichlet energy density and conflicting Dirichlet boundary conditions. For systems with constant velocity and constant pressure in confined channels of any width, we prove that OR solutions only exist for mutually orthogonal boundary conditions imposed on θ. This fact is known, but we rediscover this fact with new arguments. For all other choices of Dirichlet boundary conditions for θ, OR solutions do not exist and using geometric and comparison principles, we prove the existence of a unique, symmetric and non-singular (s, θ)-profile in these cases. For general flows with non-constant velocity and pressure, in section 4, we work with large domains ($L^* \to 0$) and compute asymptotic approximations for OR-type solutions, that exhibit a singular line or domain wall in the channel centre, for both passive and active scenarios. Our asymptotic methods are adapted from [7], where the authors investigate a chevron texture characterised specifically by a $\pm\pi/4$ jump in θ, using an Ericksen model for uniaxial NLCs with variable degree of orientation. These asymptotic methods, now placed within the Beris-Edwards framework, allow us to explicitly construct solutions characterised by an isotropic line, with a jump discontinuity in the nematic director, which we refer to as an *OR-type solution*. Though the director is not constant away from the isotropic line, as in OR solutions, the isotropic or singular line captures OR-type behavior that survives in nematodynamics. These OR-type solutions are also constructed for active nematodynamics, by working in the reduced Beris-Edwards framework with additional non-equilibrium active stresses [17], illustrating the universality of OR-type situations in equilibrium and non-equilibrium scenarios.

We validate our asymptotics and confirm the existence of OR-type solutions for passive and active nematodynamics (with non-constant pressure and flow), with extensive numerical experiments, for large and small values of L^*. In both settings, we find OR-type solutions for all values of L^*, with mutually orthogonal Dirichlet conditions for θ on the channel surfaces. OR-type solutions are stable for large L^*, and unstable for small L^*. In fact, we observe multiple unstable OR-type solutions for small values of L^*, highlighting the ubiquity of these singular solutions. Our asymptotic expansions serve as excellent initial conditions for numerically computing different branches of OR-type solutions, characterised by different jumps in θ across the singular lines, and the asymptotics agree well with the numerics. We conclude that OR-type solutions are generic for certain classes of phenomenological models, and whilst they are only observed for specific boundary conditions and they are only stable in certain geometries, unstable OR-type solutions can be stabilised by external controls and can certainly play a key role in switching and dynamical phenomena.

The paper is organised as follows. In section 2, we describe the Beris-Edwards model, our geometry and the boundary conditions. In section 3, we study flows with constant velocity and pressure, and identify conditions which allow and disallow OR solutions, in terms of the boundary conditions. In section 4, we compute asymptotic expansions for OR-type solutions with passive and active nematic flows for small L^*/large channel widths, providing explicit limiting profiles in these cases. We then supplement our analysis with detailed numerical experiments, to assess the accuracy of the asymptotics, as well as illustrate the plethora of OR-type solutions in non-equilibrium scenarios along with their non-OR counterparts. Some brief conclusions and future perspectives are given in section 5.

2. Theory. We consider NLCs sandwiched inside a three dimensional channel, $\tilde{\Omega} = \{(x, y, z) \in \mathbb{R}^3 : -D \leq x \leq D, -L \leq y \leq L, 0 \leq z \leq H\}$ where L, D, and H are the width, length and height of the channel, respectively, and we assume that $D \gg L$. For a shallow channel as considered in this manuscript, structural properties are invariant across the channel height and we therefore ignore the z-component and restrict ourselves to a two-dimensional system in the xy-plane. Furthermore, since $D \gg L$, it is reasonable to assume that the system is invariant in x, and structural properties vary in the y-direction only, leaving us with an effectively one-dimensional problem, for $y \in [-L, L]$.

There are two macroscopic variables - the fluid velocity $\mathbf{u}$, and a reduced Landau-de Gennes (LdG) $\mathbf{Q}$-tensor order parameter that measures the orientational ordering of the NLC in the xy-plane (see [19, 32] for justification of reduced models). More precisely, the reduced $\mathbf{Q}$-tensor is a symmetric traceless 2×2 matrix i.e., $\mathbf{Q} \in S_2 := \{\mathbf{Q} \in \mathbb{M}^{2\times 2} : Q_{ij} = Q_{ji}, Q_{ii} = 0\}$, which can be written as:

$$\mathbf{Q} = s\left(\mathbf{n} \otimes \mathbf{n} - \frac{\mathbf{I}}{2}\right). \tag{2.1}$$

Here, s is a scalar order parameter, $\mathbf{n}$ is the nematic director (a unit vector describing the average direction of orientational ordering in the xy-plane), and $\mathbf{I}$ is the 2×2 identity matrix. Moreover, s can be interpreted as a measure of the degree of the orientational order about $\mathbf{n}$, so that the nodal sets of s (i.e., where $s = 0$) define nematic defects in the xy-plane. As a consequence of (2.1), the two independent components of $\mathbf{Q}$ are given by

$$Q_{11} = \frac{s}{2}\cos 2\theta, \quad Q_{12} = \frac{s}{2}\sin 2\theta, \tag{2.2}$$

when $\mathbf{n} = (\cos\theta, \sin\theta)$, and θ denotes the angle between $\mathbf{n}$ and the x-axis. Conversely, applying basic trigonometric identities, we have the following relationships,

$$s = 2\sqrt{Q_{11}^2 + Q_{12}^2} \quad \text{and} \quad \theta = \frac{1}{2}\tan^{-1}\left(\frac{Q_{12}}{Q_{11}}\right). \tag{2.3}$$

We work within the Beris-Edwards framework for nematodynamics [4]. There are three governing equations: an incompressibility constraint for $\mathbf{u}$, an evolution equation for $\mathbf{u}$ (essentially the Navier–Stokes equation with an additional stress due to the nematic ordering σ), and an evolution equation for $\mathbf{Q}$ which has an additional stress induced by the fluid vorticity [28]. These equations are given below,

$$\nabla \cdot \mathbf{u} = 0, \quad \rho \frac{D\mathbf{u}}{Dt} = -\nabla p + \nabla \cdot (\mu(\nabla \mathbf{u} + (\nabla \mathbf{u})^T) + \sigma),$$
$$\frac{D\mathbf{Q}}{Dt} = \zeta \mathbf{Q} - \mathbf{Q}\zeta + \frac{1}{\gamma}\mathbf{H}.$$

Here ρ and μ are the fluid density and viscosity respectively, p is the hydrodynamic pressure, ζ is the anti-symmetric part of the velocity gradient tensor and γ is the rotational diffusion constant. The nematic stress is defined to be

$$\sigma = \mathbf{QH} - \mathbf{HQ} \quad \text{and} \quad \mathbf{H} = \kappa \nabla^2 \mathbf{Q} - A\mathbf{Q} - C|\mathbf{Q}|^2 \mathbf{Q},$$

where $\mathbf{H}$ is the molecular field related to the LdG free energy, κ is the nematic elasticity constant, $A < 0$ is a temperature dependent constant, $C > 0$ is a material dependent constant, and $|\mathbf{Q}| = \sqrt{\mathrm{Tr}(\mathbf{Q}^T\mathbf{Q})}$, is the Frobenius norm. Finally, we assume that all quantities depend on y alone and work with a unidirectional channel flow, so that $\mathbf{u} = (u(y), 0)$. The incompressibility constraint is automatically satisfied. To render the equations nondimensional, we use the following scalings, as in [28],

$$y = L\tilde{y},\ t = \frac{\gamma L^2}{\kappa}\tilde{t},\ u = \frac{\kappa}{\gamma L}\tilde{u},\ Q_{11} = \sqrt{\frac{-2A}{C}}\tilde{Q}_{11},\ Q_{12} = \sqrt{\frac{-2A}{C}}\tilde{Q}_{12},\ p_x = \frac{\mu\kappa}{\gamma L^3}\tilde{p}_x,$$

and then drop the tilde for simplicity. Our rescaled domain is $\Omega = [-1, 1]$ and the evolution equations become

(2.4a) $$\frac{\partial Q_{11}}{\partial t} = u_y Q_{12} + Q_{11,yy} + \frac{1}{L^*}Q_{11}(1 - 4(Q_{11}^2 + Q_{12}^2)),$$

(2.4b) $$\frac{\partial Q_{12}}{\partial t} = -u_y Q_{11} + Q_{12,yy} + \frac{1}{L^*}Q_{12}(1 - 4(Q_{11}^2 + Q_{12}^2)),$$

(2.4c) $$L_1 \frac{\partial u}{\partial t} = -p_x + u_{yy} + 2L_2(Q_{11}Q_{12,yy} - Q_{12}Q_{11,yy})_y,$$

where $L_1 = \frac{\rho\kappa}{\mu\gamma}$, $L^* = \frac{-\kappa}{AL^2}$, and $L_2 = \frac{-2A\gamma}{C\mu} = \frac{-2AEr^*}{CEr}$ are dimensionless parameters. Here, Er is the Ericksen number and $Er^* = u_0 L\gamma/\kappa$ is analogous to the Ericksen number in terms of the rotational diffusion constant γ, rather than viscosity μ. We interpret L^* as a measure of the domain size i.e. it is the square of the ratio of two length scales: the nematic correlation length, $\xi = \sqrt{-\kappa/A}$ for $A < 0$ and the domain size L, so that the $L^* \to 0$ limit is relevant for large channels or macroscopic domains. The parameter, L_2 is the product of the ratio of material and temperature-dependent constants and the ratio of rotational to momentum diffusion [28]. Analytically, we focus on the static problem. However, we use gradient flow methods to numerically solve (2.4) in order to compute solutions of the static problem. We therefore fix $L_1 = 1$, and as such do not comment on its physical significance. The static governing equations for (s, θ), can be obtained from (2.4) using (2.2):

(2.5a) $$s_{yy} = 4s\theta_y^2 + \frac{1}{L^*}s(s^2 - 1),$$

(2.5b) $$s\theta_{yy} = \frac{1}{2}su_y - 2s_y\theta_y,$$

(2.5c) $$u_{yy} = p_x - L_2(s^2\theta_y)_{yy}.$$

The formulation in terms of (s, θ) gives informative insight into the solution profiles and avoids some of the degeneracy conditions coded in the $\mathbf{Q}$-formulation.

We work with Dirichlet conditions for (s, θ) as given below:

$$s(-1) = s(1) = 1, \tag{2.6a}$$

$$\theta(-1) = -\omega\pi,\ \theta(1) = \omega\pi, \tag{2.6b}$$

where $\omega \in \left[-\frac{1}{2}, \frac{1}{2}\right]$, is the winding number. This translates to the following boundary conditions for $\mathbf{Q}$:

$$Q_{11}(\pm 1) = \frac{1}{2}\cos(2\omega\pi),\ Q_{12}(-1) = -\frac{1}{2}\sin(2\omega\pi),\ Q_{12}(1) = \frac{1}{2}\sin(2\omega\pi). \tag{2.7}$$

The boundary conditions in (2.6a) imply that the nematic molecules are perfectly ordered on the bounding plates. We consider asymmetric Dirichlet boundary conditions in (2.6b) for the angle θ. A potential issue follows from (2.3): the range of θ is $(-\frac{\pi}{4}, \frac{\pi}{4})$, but our boundary conditions extend to $\pm\frac{\pi}{2}$. However, we circumvent this issue by using the function $\text{atan2}(y, x) \in (-\pi, \pi]$, which returns the angle between the line connecting the point (x, y) to the origin and the positive x axis.

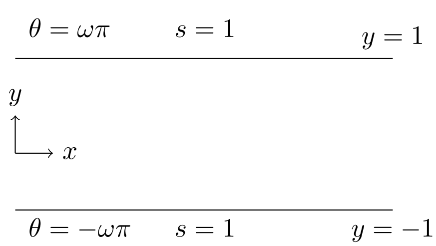

Fig. 1. *Boundary conditions for s and θ.*

For the flow field, we consider the typical no-slip boundary conditions, namely

$$u(-1) = u(1) = 0, \tag{2.8}$$

and assume that the pressure p is uniform in the y-direction, hence it depends on x only.

3. Passive flows with constant velocity and pressure. In this section, we study nematic flows with constant velocity and pressure without additional activity. This framework, though somewhat artificial, allows for OR solutions, although OR-type solutions exist in more generic situations with non-constant flows (as we show in subsequent sections). We work with both the $\mathbf{Q}$- and (s, θ)-frameworks in this section.

We interpret OR solutions as solutions of (2.4) with polydomain structures: a polydomain is a sub-domain with constant nematic director profiles, separated by domain walls to account for jumps in the nematic director across polydomain boundaries. In the (s, θ)-formulation and our one-dimensional framework, OR solutions correspond to a partition of the domain $\Omega = [-1, 1]$ into sub-domains, $\Omega = \sum_{j=1}^{n} \Omega_j$, where each Ω_j is a *polydomain*. The polydomains correspond to intervals with constant θ (recall that θ is the orientation of $\mathbf{n}$), and the domain wall is described by a point with $s = 0$, to regularise the jump in θ between polydomains. In three-dimensions (3D), the polydomains correspond to 3D cuboidal regions and the domain walls are singular surfaces in θ. OR-type solutions are simply interpreted as solutions of (2.4) that have a non-empty nodal set for s or exhibit domain walls, without the constraint of constant θ or the existence of polydomains. In the $\mathbf{Q}$-framework, OR solutions have a distinct but less obvious signatures. The domain walls correspond to the nodal set of the $\mathbf{Q}$-tensor order parameter, but polydomains are only compatible with specific boundary conditions, as we show in the following results.

OR solutions are characterised by sub-intervals with constant θ, separated by nodal points with $s = 0$. From (2.5b), constant θ implies constant fluid velocity u and from (2.5c), constant pressure, p. Therefore, in order to study OR solutions, we assume constant velocity and pressure to start with. As such, we let $'$ denote differentiation with respect to y in this section.

In this scenario the static version of (2.4a)-(2.4b) is

$$Q_{11}'' = \frac{1}{L^*} Q_{11}(4(Q_{11}^2 + 4Q_{12}^2) - 1), \tag{3.1a}$$

$$Q_{12}'' = \frac{1}{L^*} Q_{12}(4(Q_{11}^2 + 4Q_{12}^2) - 1). \tag{3.1b}$$

From these equations it follows that (2.4c) is satisfied. The equations (3.1a)-(3.1b) are the Euler-Lagrange equations associated with the energy

(3.2)
$$F_{LG}[Q_{11}, Q_{12}] = \int_\Omega \left((Q_{11}')^2 + (Q_{12}')^2 \right) + \frac{1}{L^*}(Q_{11}^2 + Q_{12}^2)(2(Q_{11}^2 + Q_{12}^2) - 1) \, \mathrm{d}y.$$

The admissible $\mathbf{Q}$-tensors belong to the Sobolev space, $W^{1,2}([-1,1]; S_2)$, where S_2 is the space of symmetric and traceless 2×2 matrices, subject to appropriately defined boundary conditions (see (2.7)). The stable and physically observable configurations correspond to local or global minimizers of (3.2), in the prescribed admissible space.

In the static case, with constant u and p, the corresponding equations for (s, θ) can be deduced from (2.5a), (2.5b) :

$$s'' = 4s(\theta')^2 + \frac{1}{L^*} s(s^2 - 1), \tag{3.3a}$$

$$\left(s^2\theta'\right)' = 0, \implies s^2\theta' = B, \tag{3.3b}$$

whilst (2.5c) is automatically satisfied. In the above, B is a fixed constant of integration; in fact

$$B = \theta'(-1) = \theta'(1). \tag{3.4}$$

When $\omega \geq 0$ and recalling the boundary conditions for θ, there exists a point y_0 such that $\theta'(y_0) \geq 0$, hence $B \geq 0$, and $\theta' \geq 0$ for all $y \in [-1, 1]$. Thus, we have

$$-\omega\pi \leq \theta \leq \omega\pi, \ \forall y \in [-1, 1] \text{ and } \forall \omega \in \left[0, \frac{1}{2}\right]. \tag{3.5}$$

Similar comments apply when $\omega \leq 0$, for which $B \leq 0$, and $\theta' \leq 0$ for all $y \in [-1, 1]$. If $B = 0$, we either have $s = 0$ or θ=constant almost everywhere, compatible with the definition of an OR solution (unless $\omega = 0$, and $(s, \theta) = (1, 0)$, which is not an OR solution). Conversely, an OR solution, by definition, has $B = 0$ since polydomain structures correspond to piecewise constant θ-profiles. In other words, if $\omega \neq 0$, OR solutions exist if and only if $B = 0$. If $B \neq 0$, then OR solutions are necessarily disallowed because a non-zero value of B implies that $s \neq 0$ on Ω. The following results show that the choice of B is in turn dictated by ω, or the Dirichlet boundary conditions, and this sheds beautiful insight into the how the boundary datum manifests in the multiplicity and regularity of solutions. In what follows, we let $\epsilon := \frac{1}{L^*}$, so that $\epsilon \propto L^2$ where L is the physical channel width.

Note that (3.3a) and (3.3b) are the Euler-Lagrange equations of the following energy,

$$F_{LG}[s,\theta] = \int_\Omega \left(\frac{(s')^2}{4} + s^2(\theta')^2 \right) + \frac{\epsilon s^2}{4}\left(\frac{s^2}{2} - 1\right) \,\mathrm{d}y, \tag{3.6}$$

but we only consider $(s,\theta) \in W^{1,2}(\Omega;\mathbb{R})$ and focus on smooth, classical solutions of (3.3a) and (3.3b), subject to the boundary conditions in (2.6a)-(2.6b), and not OR solutions. We first prove that OR solutions only exist for the special values, $\omega = \pm\frac{1}{4}$, in the $\mathbf{Q}$-framework. If $\omega = \pm\frac{1}{4}$, then B can be either zero or non-zero for different solution branches, especially for small values of ϵ that admit multiple solution branches. Once the correspondence between ω, B and OR solutions is established, we proceed to prove several qualitative properties of the corresponding (s,θ)-profiles which are of independent interest, followed by some asymptotic analysis and numerical experiments (see supplementary material).

Theorem 3.1. *For all $\epsilon \geq 0$, there exists a minimiser of the energy (3.2), in the admissible space*

$$\mathcal{A} = \Bigg\{ \mathbf{Q} \in W^{1,2}([-1,1];S_2)\,;Q_{11}(\pm 1) = \frac{\cos(2\omega\pi)}{2}, \\ Q_{12}(-1) = -\frac{\sin 2\omega\pi}{2}, Q_{12}(1) = \frac{\sin 2\omega\pi}{2} \Bigg\}. \tag{3.7}$$

Moreover, the system (3.1) admits an analytic solution for all $\epsilon \geq 0$, in $\mathcal{A}$. OR solutions only exist for $\omega = \pm\frac{1}{4}$ in (2.7).

Proof. The existence of an energy minimizer for (3.2) in $\mathcal{A}$, is immediate from the direct methods in the calculus of variations, for all ϵ and ω, and the minimizer is a classical solution of the associated Euler-Lagrange equations (3.1), for all ϵ and ω. In fact, using standard arguments in elliptic regularity, one can show that all solutions of the system (3.1) are analytic [5].

The key observation is

$$(Q_{12}'Q_{11} - Q_{11}'Q_{12})' = Q_{12}''Q_{11} + Q_{12}'Q_{11}' - Q_{12}'Q_{11}' - Q_{12}Q_{11}'' = 0,$$

and hence, $Q_{12}'Q_{11} - Q_{11}'Q_{12}$ is a constant. In fact, using (2.3), we see that

$$(s^2\theta')' = 2(Q_{12}''Q_{11} - Q_{11}''Q_{12}) = 0 \implies s^2\theta' = 2(Q_{12}'Q_{11} - Q_{11}'Q_{12}) = B,$$

where B is as in (2.5b). Now let $B = 0$ (so that OR solutions are possible), then

$$Q_{12}'Q_{11} = Q_{11}'Q_{12} \text{ for all } y \in [-1,1]. \tag{3.8}$$

There are two obvious solutions of (3.8) i.e. $Q_{11} \equiv 0$ (i.e., $\omega = \pm\frac{1}{4}$), or $Q_{12} \equiv 0$ (i.e., $\omega = 0, \pm\frac{1}{2}$), everywhere on Ω.

For the case $Q_{12} \equiv 0$ and $\omega = \pm\frac{1}{2}$, the $\mathbf{Q}$ Euler-Lagrange equations reduce to

$$\begin{cases} Q_{11}'' = \epsilon Q_{11}(4Q_{11}^2 - 1), \\ Q_{11}(-1) = -\frac{1}{2},\ Q_{11}(1) = -\frac{1}{2}. \end{cases} \tag{3.9}$$

This is essentially the ODE considered in equation (20) of [23]. Applying the arguments in Lemma 5.4 of [23], the solution Q_{11} of (3.9) must satisfy $Q_{11}'(-1) = 0$, or Q_{11}' is always positive. However, the latter is not possible since we have symmetric boundary conditions. Hence, when $\omega = \pm\frac{1}{2}$, the unique solution to (3.9) is the constant solution $(Q_{11}, Q_{12}) = (-\frac{1}{2}, 0)$. This corresponds to $s = 1$ everywhere in Ω, inconsistent with an OR solution. The same arguments apply to the case $Q_{12} \equiv 0$ and $\omega = 0$. In this case the boundary conditions are $Q_{11}(\pm 1) = \frac{1}{2}$, and the corresponding (s, θ) solution is simply, $(s, \theta) = (1, 0)$. Again, this is not an OR solution.

When $Q_{11} \equiv 0$ $(\omega = \pm\frac{1}{4})$, the $\mathbf{Q}$ system becomes

$$\begin{cases} Q_{12}'' = \epsilon Q_{12}(4Q_{12}^2 - 1), \\ Q_{12}(-1) = -\frac{1}{2},\ Q_{12}(1) = \frac{1}{2}. \end{cases} \tag{3.10}$$

Applying the arguments in Lemma 5.4 of [23], we see (3.10) has a unique solution which is odd and increasing, with a single zero at $y = 0$ - the centre of the channel. This is an OR solution, since $Q_{11} = 0$ implies that θ is necessarily constant on either side of $y = 0$.

It remains to show that there are no solutions (Q_{11}, Q_{12}) of (3.1), which satisfy (3.8), other than the possibilities considered above. To this end, we assume that we have non-trivial solutions, Q_{11} and Q_{12} such that (3.8) holds. We recall that all solution pairs, (Q_{11}, Q_{12}) of (3.1) are analytic and hence, can only have zeroes at isolated interior points of $\Omega = [-1, 1]$. This means that there exists a finite number of intervals $(-1, y_1), \ldots, (y_n, 1)$, such that $Q_{11} \neq 0$ and $Q_{12} \neq 0$ in the interior of these intervals, whilst either $Q_{11}(y_i)$, $Q_{12}(y_i)$, or both, equal zero at each intervals end-points. We then have that

$$\frac{Q_{12}'}{Q_{12}} = \frac{Q_{11}'}{Q_{11}} \implies |Q_{11}| = c_i |Q_{12}| \text{ for } y \in (y_{i-1}, y_i)$$

for constants $c_i > 0$ and $i = 1, \ldots, n$. Therefore, there exists an interval, (y_{i-1}, y_i), for which Q_{11} and Q_{12} have the same, or opposite signs. Assume without loss of generality (W.L.O.G.) Q_{11} and Q_{12} have the same sign, then the analytic function

$$f(y) := Q_{11}(y) - c_i Q_{12}(y) = 0, \text{ for } y \in (y_{i-1}, y_i).$$

Therefore, $f(y) = 0$ for all $y \in [-1, 1]$. Evaluating at $y = \pm 1$, we have

$$\cos(2\omega\pi) = -\sin(2\omega\pi)c_i \text{ and } \cos(2\omega\pi) = \sin(2\omega\pi)c_i,$$

and this is only possible if $\cos(2\omega\pi) = 0$ and $\sin(2\omega\pi)c_i = 0$, which implies $\omega = \pm\frac{1}{4}$ and $c_i = 0$. Hence, there are only three possibilities for $\omega = 0, \pm\frac{1}{4}, \pm\frac{1}{2}$ that are consistent with (3.8), of which OR solutions are only compatible with $\omega = \pm\frac{1}{4}$. □

In what follows, we consider the solution profiles, (s, θ) of (3.3a) and (3.3b), from which we can construct a solution of the system (3.1), using the definitions (2.2). The first proposition below is adapted from results in [26], although some additional work is needed to deal with the positivity of s. The proof is given in the supplementary material.

THEOREM 3.2. *(Maximum Principle) Let s and θ be solutions of (3.3a) and (3.3b), where s is at least C^1, then*

$$0 < s \leq 1 \quad \forall y \in [-1,1]. \tag{3.11}$$

Proof. See supplementary material. ∎

For the next batch of results, we omit the case $B = 0$ and focus on the (s,θ)-profiles of non OR-solutions, which are necessarily smooth. We exploit this fact to prove that there exists a unique solution pair, (s,θ) of (3.3), such that s has a symmetric even profile about $y = 0$, for every $B \neq 0$.

THEOREM 3.3. *Any non-constant and non-OR solution, s, of the Euler-Lagrange equations (3.3), has a single critical point which is necessarily a non-trivial global minimum at some $y^* \in (-1,1)$.*

Proof. For clarity, we denote a specific solution of (3.3a) and (3.3b), by (s_{sol}, θ_{sol}) in this proof. Recall that for non-OR solutions, we necessarily have $B = \theta'(\pm 1) \neq 0$ and $s \neq 0$ anywhere. Using the definition of B in (3.3), we have

$$s'' = \frac{4B^2}{s^3} + \epsilon(s^3 - s). \tag{3.12}$$

The right hand side of (3.12) is well defined and continuous for $s \in (0,1]$, and as such, a solution, s_{sol}, will be C^2. In fact, the right hand side of (3.12) is smooth, hence any solution, s_{sol}, will be smooth.

The boundary conditions, $s(\pm 1) = 1$, imply that a non-trivial solution has $s'_{sol}(y^*) = 0$ for some $y^* \in [-1,1]$, where s' is defined as,

$$s' = \pm\sqrt{\left(-4B^2 s^{-2} + \epsilon\left(\frac{s^4}{2} - s^2\right) + A\right)}. \tag{3.13}$$

Here, A is a constant of integration and $A = 4B^2 + \frac{\epsilon}{2} + s'(\pm 1)^2$, hence, we must have

$$A \geq 4B^2 + \frac{\epsilon}{2}. \tag{3.14}$$

Since s' is defined in terms of s and not y, solutions of $s' = 0$ give us the extrema of a solution s_{sol} (i.e., maxima or minima), rather than the location of the critical points on the y-axis. The condition $s' = 0$ is equivalent to

$$A = 4B^2 s^{-2} - \epsilon\left(\frac{s^4}{2} - s^2\right). \tag{3.15}$$

Clearly if $\epsilon = 0$, we can only have one extremum, namely $s = \sqrt{\frac{4B^2}{A}}$, which in view of the boundary conditions and maximum principle, must be a minimum. For $\epsilon > 0$, solving (3.15) is equivalent to computing the roots of $f(s) = 0$ where

$$f(s) := s^6 - 2s^4 + \frac{2A}{\epsilon}s^2 - \frac{8B^2}{\epsilon}. \tag{3.16}$$

Firstly, note that f has a root for $s \in (0,1]$, since $f(0) = \frac{-8B^2}{\epsilon} < 0$ and $f(1) = -1 + \frac{2A}{\epsilon} - \frac{8B^2}{\epsilon} \geq 0$, by (3.14). Differentiating (3.16), we obtain

$$\frac{df}{ds}(s) = 6s^5 - 8s^3 + \frac{4A}{\epsilon}s,$$

and the critical points of f are given by

$$s = 0,\ s_{\pm} = \sqrt{\frac{8 \pm \sqrt{64 - \frac{96A}{\epsilon}}}{12}}, \tag{3.17}$$

provided that $A \leq \frac{2}{3}\epsilon$. There are now three cases to consider.

Case 1: If $A > \frac{2}{3}\epsilon$, $f(s)$ has one critical point at $s = 0$, which is a negative global minimum. Hence, f has one root in the range, $s \in (0, 1]$.

Case 2: Let $A = \frac{2}{3}\epsilon$, so that the two critical points $s_{\pm}$ coincide. The point $s = 0$ is still a minimum of $f(s)$ and the coefficient of s^6 is positive (so $f \to \infty$ as $s \to \infty$), so we deduce that $s_{\pm}$ is a stationary point of inflection (this can be checked via direct computation). So again, f has one root for $s \in (0, 1]$.

Case 3: Finally, let $A < \frac{2}{3}\epsilon$, so that $s_{\pm}$ are distinct critical points of f. The point, $s = 0$, is still a minimum of $f(s)$ and the coefficient of s^6 is positive, so that there are two possibilities: (a) $s_{\pm}$ are distinct saddle points, and since f is increasing for $s > 0$, we see f has a single root for $s \in (0, 1]$, or (b) s_- is a local maximum and s_+ is a local minimum of $f(s)$. In the latter case, $s = 0$ is still a global minimum for $f(s)$, because $f(s_+) > f(0)$. Using this information, we can produce a sketch of $f(s)$ (shown in Figure 2), and there are 5 cases to consider for the number of roots of f.

In cases (i) and (v) of Figure 2, f has only one root for $s \in (0, 1]$. Next, in order for the derivative s'_{sol} to be real, the term under the square root in (3.13), has to be non-negative. This requires that $f(s) \geq 0$ for all $s \in [c, 1]$, for some $c > 0$. Applying this argument to cases (ii) and (iii) in Figure 2 by omitting regions with $f(s) < 0$, we deduce that f has a single non-trivial root for $s \in (0, 1]$.

For case (iv), we have two distinct roots in an interval such that $f(s) \geq 0$, one of which is s_+, and the other root is labelled as s_1. Recalling that s_+ is also a solution of $f'(s) = 0$, we deduce that s_+ is a repeated root of f. Then, f can be factorised as:

$$\begin{aligned} f(s) &= (s - s_+)^2(s + s_+)^2(s - s_1)(s + s_1) \\ &= s^6 - (2s_+^2 + s_1^2)s^4 + (s_+^4 + 2s_1^2 s_+^2)s^2 - s_1^2 s_+^4. \end{aligned} \tag{3.18}$$

Comparing the coefficient of s^4 and s^0 in (3.16), with (3.18), we have $s_1^2 = 2(1 - s_+^2)$ and $s_1^2 = \frac{8B^2}{\epsilon s_+^4}$, which implies

$$4B^2 + \epsilon s_+^4 (s_+^2 - 1) = 0. \tag{3.19}$$

Comparing (3.12) with (3.19), we deduce that, $s''(s_+) = 0$. By the uniqueness theory for Cauchy problems, this implies that $s_{sol} \equiv s_+$, which is inadmissible and this case is excluded.

In cases 1, 2 and 3 we have demonstrated that s_{sol} has a unique positive critical value, which must be the minimum value, and in case 3, we have a lower bound for the minimum value i.e. $s_{min} > s_+$. The unique minimum value is attained at a unique interior point (if there were two interior minima at say y^* and y^{**}, a non-constant solution would exhibit a local maximum between the two minima, which is excluded by a unique critical value for s_{sol}). This completes the proof. ∎

THEOREM 3.4. *For a given $B = \theta'(\pm 1) \neq 0$, the system (3.3), subject to the boundary conditions (2.6), has a unique solution for a fixed ϵ and ω. Hence, for any value of ω that does not permit OR solutions, the system (3.3) always has a unique solution.*

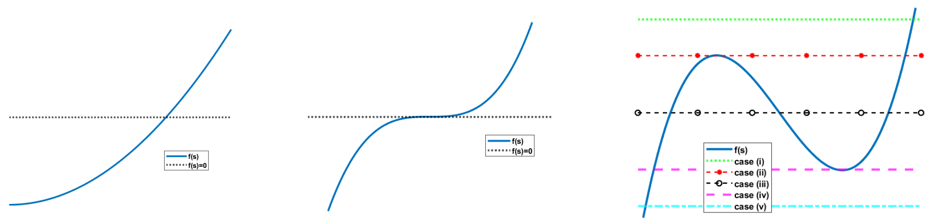

Case 1 Case 2 Case 3 (b)

FIG. 2. *The horizontal lines represent $f(s) = 0$.*

Proof. Recall, for $\omega \neq 0$, OR solutions exist if and only if $B = 0$. When $\omega = 0$, (3.3b) implies we must have $B = 0$, the proof of Theorem 3.2 (see supplementary material) then shows the unique solution in $W^{1,2}$ is $(s, \theta) = (1, 0)$. Hence, for $\omega = 0$, we can only have non-uniqueness if an OR solution exists.

For $B \neq 0$, the system (3.3) can be written as

$$s'' = \frac{4B^2}{s^3} + \epsilon s(s^2 - 1), \tag{3.20a}$$

$$s^2\theta' = B. \tag{3.20b}$$

Throughout this proof we take $B > 0$, so that $s \neq 0$ and hence, the right hand side of (3.20a) is analytic. The case $B < 0$ can be tackled in the same manner.

In the first step, we show that (3.20) has a unique solution for fixed B, ϵ and ω. Assume for contradiction that (s_1, θ_1) and (s_2, θ_2) are distinct solutions pairs of (3.20), which satisfy (2.6). As such, they must have distinct derivatives at $y = -1$ (otherwise they would satisfy the same Cauchy problem). Suppose W.L.O.G.

$$s_1'(-1) < s_2'(-1) \leq 0. \tag{3.21}$$

Since $s_1(1) = s_2(1) = 1$, there exists $y_0 = \min\{y > -1 : s_1(y_0) = s_2(y_0) := s_0\}$. Therefore, $s_1 < s_2$ for all $y \in (-1, y_0)$. Further, since s_1 and s_2 have one non-trivial global minimum (Theorem 3.3), there are four possibilities for the location of y_0: (i) Case I: $y_0 = 1$; (ii) Case II: $y_0 < \min\{\alpha, \beta\}$ where s_1 attains its unique minimum at $y = \alpha$ and s_2 attains its unique minimum at $y = \beta$; (iii) Case III: $\alpha \leq y_0 \leq \beta$, or $\beta \leq y_0 \leq \alpha$; and (iv) Case IV: $y_0 > \max\{\alpha, \beta\}$. In case I, $s_1 < s_2$ implies $\theta_1' > \theta_2'$ for all $y \in (-1, 1)$, since both solution pairs satisfy (3.20b). Hence, $\theta_1(y) - \theta_2(y)$ is increasing, and cannot vanish at $y = 1$, contradicting the boundary condition at $y = 1$.

For Case II, we have

$$s_2'(y_0) \leq s_1'(y_0) < 0$$

so that

$$(s_2'(-1))^2 - (s_2'(y_0))^2 < (s_1'(-1))^2 - (s_1'(y_0))^2.$$

Using (3.13), this is equivalent to

$$-4B^2-\frac{\epsilon}{2}+A_2-\left(-\frac{4B^2}{s_0^2}+\epsilon s_0^2\left(\frac{s_0^2}{2}-1\right)+A_2\right)<$$
$$-4B^2-\frac{\epsilon}{2}+A_1-\left(-\frac{4B^2}{s_0^2}+\epsilon s_0^2\left(\frac{s_0^2}{2}-1\right)+A_1\right),$$

where A_1 and A_2 are constants of integration associated with s_1 and s_2 respectively, and may not be equal. However, the left and right hand sides are in fact equal, yielding the desired contradiction.

For Cases III and IV, there must exist another point of intersection, $y=y_1\in(\max\{\alpha,\beta\},1]$, such that

$$(s_1-s_2)(y_1)=0;\quad (s_1-s_2)'(y_1)<0$$

and

$$0<s_1'(y_1)\leq s_2'(y_1).$$

In this case, we can use

$$(s_2'(-1))^2-(s_2'(y_1))^2<(s_1'(-1))^2-(s_1'(y_1))^2$$

to get the desired contradiction. We therefore conclude that for fixed B, ϵ and ω, the solution of (3.3) is unique.

Next, we show the constant B, is unique for fixed ϵ and ω. We assume that there exist two distinct solution pairs, (s_1,θ_1) and (s_2,θ_2), which by the first part of the proof, are the unique solutions of

$$s_1''=\frac{4B_1^2}{s_1^3}+\epsilon s_1(s_1^2-1),\quad s_2''=\frac{4B_2^2}{s_2^3}+\epsilon s_2(s_2^2-1)$$

and

$$s_1^2\theta_1'=B_1,\quad s_2^2\theta_2'=B_2,$$

respectively, subject to (2.6), for the same value of ω. Let $0<B_1\leq B_2$. Using a change of variable $u_k=1-s_k\in[0,1)$, for $k=1,2$ so that $u_k(\pm1)=0$, we can use the method of sub- and supersolutions to deduce that

$$s_2\leq s_1 \text{ for all } y\in[-1,1]. \tag{3.22}$$

This implies

$$\theta_1'=\frac{B_1}{s_1^2}\leq\frac{B_2}{s_2^2}=\theta_2'\quad\forall y\in[-1,1]. \tag{3.23}$$

If $\theta_1'<\theta_2'$ anywhere, then $\theta_1(1)=\omega\pi$ does not hold, hence we must have equality i.e., $\theta_1'=\theta_2'$. It therefore follows that $B_1s_2^2=B_2s_1^2$, but the boundary conditions necessitate that $B_1=B_2:=B$ and hence, $s_1=s_2:=s$. Finally, integrating $\theta_1'=B/s^2$, it follows that θ_1 is unique and is given by

$$\theta_1(y)=\omega\pi-\int_y^1\frac{B}{s^2}\,\mathrm{d}y,\ \text{where } B=2\omega\pi\left(\int_{-1}^1\frac{1}{s^2}\,\mathrm{d}y\right)^{-1}. \tag{3.24}$$

The preceding arguments show that $\theta_1=\theta_2$ and the proof is complete. ∎

THEOREM 3.5. *For $B = \theta'(\pm 1) \neq 0$, the unique solution, (s, θ) of (3.3), has the following symmetry properties:*

$$s(y) = s(-y) \qquad \theta(y) = -\theta(-y)$$

for all $y \in [-1, 1]$. Then s has a unique non-trivial minimum at $y = 0$.

Proof. It can be readily checked that for $B \neq 0$, the system of equations (3.3) admits a solution pair, (s, θ) such that s is even, and θ is odd for $y \in [-1, 1]$, compatible with the boundary conditions. Combining this observation with the uniqueness result for $B \neq 0$, the conclusion of the theorem follows. □

The preceding results apply to non OR-solutions. OR solution-branches have been studied in detail, in a one-dimensional setting, in the **Q**-framework [23]. Using the arguments in [23], one can prove that for $\omega = \pm\frac{1}{4}$, OR solutions exist for all $\epsilon \geq 0$ and are globally stable as $\epsilon \to 0$, but lose stability as ϵ increases. In particular, non-OR solutions emerge as ϵ increases, for $\omega = \pm\frac{1}{4}$, and these non-OR solutions do not have polydomain structures. More precisely, we can explicitly compute limiting profiles in the $\epsilon \to 0$ an $\epsilon \to \infty$ limits. In the $\epsilon \to 0$ limit, relevant for nano-scale channels (also see [21]), the limiting problem can be solved explicitly in the **Q**-framework and the associated (s, θ) profiles are extracted using (2.3). Recall the system (3.1). From the maximum principle, $||\mathbf{Q}||_{L^\infty}$ is bounded independently of ϵ, and the system (3.1) reduces to the Laplace equations in the $\epsilon \to 0$ limit [15]:

$$Q_{11}'' = 0, \quad Q_{12}'' = 0.$$

This limiting system, subject to (2.7), admits the unique solution

$$Q_{11}(y) = \frac{1}{2}\cos(2\omega\pi),\ Q_{12}(y) = \frac{y}{2}\sin(2\omega\pi). \tag{3.25}$$

Substituting (3.25) into (2.3), we obtain the following limiting profiles for s and θ, in the $\epsilon \to 0$ limit:

$$s_{0,\omega} = \sqrt{\cos^2(2\omega\pi) + y^2\sin^2(2\omega\pi)}, \tag{3.26a}$$

$$\theta_{0,\omega} = \frac{1}{2}\text{atan2}(y\sin(2\omega\pi), \cos(2\omega\pi)). \tag{3.26b}$$

Using the explicit expressions above, one can easily verify that $s_{0,\omega}$ has exactly one critical point at $y = 0$, which is a global minimum. Further, $s_{0,\pm\frac{1}{4}}(0) = 0$ and $s_{0,\omega}(0) > 0$ for $\omega \neq \pm\frac{1}{4}$.

In the $\epsilon \to \infty$ limit (relevant for micron-scale channels), the system (3.3) reduces to (see [6] for rigorous arguments)

$$s(s^2 - 1) = 0, \quad s^2\theta_y = B, \tag{3.27}$$

which, subject to the boundary conditions (2.6b), has the solution

$$s(y) = 1, \quad \theta(y) = \omega\pi y \quad \text{for all } \omega\text{, including } \omega = \pm\frac{1}{4}. \tag{3.28}$$

This asymptotic analysis is complemented by additional calculations, as well as numerical solutions of the **Q**-Euler-Lagrange equations (3.1a) and (3.1b) (along with the corresponding (s, θ) profiles), in the supplementary material.

4. Passive and Active flows. In this section, we compute asymptotic expansions for OR-type solutions of the system (2.5), in the $L^* \to 0$ limit ($\epsilon \to \infty$ limit) relevant to micron-scale channels. We consider conventional passive nematodynamics and active nematodynamics (with additional active stresses generated by internal activity), and generic scenarios with non-constant velocity and pressure. We follow the asymptotic methods in [7], to construct OR-type solutions, strongly reminiscent of chevron patterns seen in experiments [1, 11]. Recall an OR-type solution is simply a solution of (2.5) with a non-empty nodal set for the scalar order parameter, such that θ has a jump discontinuity at the zeroes of s. Unlike OR solutions, OR-type solutions need not have polydomains with constant θ-profiles.

4.1. Asymptotics for OR-type solutions in passive nematodynamics, in the $L^* \to 0$ limit. Consider the system of coupled equations, (2.5), in the $L^* \to 0$ limit. Motivated by the results of section 3, and for simplicity, we assume s attains a single minimum at $y = 0$, s is even and θ is odd, throughout this section. The first step is to calculate the flow gradient u_y. We multiply (2.5b) by s^2 so that

$$(s^2\theta_y)_y = \frac{s^2}{2}u_y. \tag{4.1}$$

Substituting $(s^2\theta_y)_y$ from (4.1) into (2.5c), we obtain

$$\left(u_y + \frac{L_2}{2}s^2 u_y\right)_y = p_x. \tag{4.2}$$

Both sides of (4.2) equal a constant, since the left hand side is independent of x, and p_x is independent of y. Integrating (4.2), we find

$$u_y = \frac{p_x y}{g(s)} + \frac{B_0}{g(s)}, \tag{4.3}$$

where B_0 is another constant and

$$g(s) = 1 + \frac{L_2}{2}s^2 > 0, \ \forall s \in \mathbb{R}. \tag{4.4}$$

Integrating (4.3), we have

$$u(y) = \int_{-1}^{y} \frac{p_x Y}{g(s(Y))} + \frac{B_0}{g(s(Y))} \, \mathrm{d}Y, \tag{4.5}$$

since $u(-1) = 0$ from (2.8). Using the no-slip condition, $u(1) = 0$ and the fact that $\int_{-1}^{1} \frac{Y}{g(s(Y))} \, \mathrm{d}Y = 0$, we see $B_0 = 0$ so that the flow velocity is given by

$$u(y) = \int_{-1}^{y} \frac{p_x Y}{g(s(Y))} \, \mathrm{d}Y, \tag{4.6}$$

and the corresponding velocity gradient is

$$u_y(y) = \frac{p_x y}{g(s)}. \tag{4.7}$$

Following the method in [7], we seek the following asymptotic expansions for (s, θ):

$$s(y) = S(y) + IS(\lambda) + \mathcal{O}(L^*), \tag{4.8a}$$

$$\theta(y) = \Theta(y) + I\Theta(\lambda) + \mathcal{O}(L^*), \tag{4.8b}$$

where S, Θ represent the outer solutions away from the jump point at $y = 0$, $IS, I\Theta$ represent the inner solutions around $y = 0$, and λ is our inner variable. Substituting these expansions into (2.5a) and (2.5b) yields

$$L^* S_{yy} + L^* IS_{yy} = 4L^*(S + IS)(\Theta_y + I\Theta_y)^2 + (S + IS)((S + IS)^2 - 1), \tag{4.9a}$$

$$(S + IS)(\Theta_{yy} + I\Theta_{yy}) = \frac{1}{2}(S + IS)u_y(y) - 2(S_y + IS_y)(\Theta_y + I\Theta_y). \tag{4.9b}$$

It is clear that (4.9a) is a singular problem in the $L^* \to 0$ limit, and as such we rescale y and set

$$\lambda = \frac{y}{\sqrt{L^*}}, \tag{4.10}$$

to be our inner variable.

The outer solution is simply the solution of (4.9a) and (4.9b), away from $y = 0$, for $L^* = 0$ and when internal contributions are ignored. In this case, (4.9a) reduces to

$$S(S^2 - 1) = 0, \tag{4.11}$$

which implies

$$S(y) = 1, \quad \text{for } y \in [-1, 0) \cap (0, 1] \tag{4.12}$$

is the outer solution. Here we have ignored the trivial solution $S = 0$, and $S = -1$, as these solutions do not satisfy the boundary conditions.

Ignoring internal contributions, (4.9b) reduces to

$$\Theta_{yy}(y) = \frac{1}{2}u_y(y) \quad \text{for } y \in [-1, 0) \cap (0, 1]. \tag{4.13}$$

From the above, $s = 1$ for $y \in [-1, 0) \cap (0, 1]$, so integrating (4.7) and imposing the no-slip boundary conditions (2.8), we obtain

$$u(y) = \frac{p_x}{2 + L_2}(y^2 - 1). \tag{4.14}$$

We take $u(0) = -\frac{p_x}{2+L_2}$, consistent with the above expression. Solving for $0 < y \leq 1$, we integrate (4.13) to obtain

$$\Theta_y(y) = \int_0^y \frac{u_y(Y)}{2}\, dY + \Theta_y(0+)$$

$$\implies \Theta_y(y) = \frac{u(y) - u(0)}{2} + \Theta_y(0+). \tag{4.15}$$

Similarly, for $-1 \leq y < 0$, integrating (4.13) yields

$$\Theta_y(y) = \frac{u(y) - u(0)}{2} + \Theta_y(0-). \tag{4.16}$$

Since $\Theta_y(0\pm)$ is unknown, we enforce the following boundary conditions at $y = 0$ to give us an explicitly computable expression

$$\Theta(0+) = \omega\pi - \frac{k\pi}{2},\ k \in \mathbb{Z}, \tag{4.17a}$$

$$\Theta(0-) = -\omega\pi + \frac{k\pi}{2},\ k \in \mathbb{Z}. \tag{4.17b}$$

We now justify this jump condition. In the case of constant flow and pressure, OR solutions jump by $\pm 2\omega\pi$, but OR-type solutions could have different jump conditions across the domain walls, hence the inclusion of the $\frac{k\pi}{2}$ term.

Substituting (4.14) into (4.15), integrating, and imposing the boundary conditions, we have that

$$\Theta(y) = \frac{p_x}{(2+L_2)}\left(\frac{y^3}{6} - \frac{y}{6}\right) + \frac{k\pi}{2}(y-1) + \omega\pi \quad \text{for } y \in (0,1]. \tag{4.18}$$

Analogously, (4.16) yields

$$\Theta(y) = \frac{p_x}{(2+L_2)}\left(\frac{y^3}{6} - \frac{y}{6}\right) + \frac{k\pi}{2}(y+1) - \omega\pi \quad \text{for } y \in [-1,0). \tag{4.19}$$

We now compute the inner solution. Substituting the inner variable (4.10), into (4.9a) and (4.9b), they become

$$L^* S_{yy} + I\ddot{S} = 4L^*(S+IS)\left(\Theta_y + \frac{I\dot{\Theta}}{\sqrt{L^*}}\right)^2 + (S+IS)((S+IS)^2-1),$$

$$(S+IS)(L^*\Theta_{yy} + I\ddot{\Theta}) = \frac{L^*}{2}(S+IS)u_y(\lambda\sqrt{L^*}) - 2L^*\left(S_y + \frac{I\dot{S}}{\sqrt{L^*}}\right)\left(\Theta_y + \frac{I\dot{\Theta}}{\sqrt{L^*}}\right),$$

where $\dot{()}$ denotes differentiation w.r.t λ. Letting $L^* \to 0$, we have that the leading order equations are

$$I\ddot{S} = 4(S+IS)(I\dot{\Theta})^2 + (S+IS)((S+IS)^2-1), \tag{4.20a}$$

$$(S+IS)I\ddot{\Theta} = -2I\dot{S}I\dot{\Theta}, \tag{4.20b}$$

or equivalently, after recalling $S = 1$,

$$\begin{aligned} I\ddot{S} &= 2IS + q_1(IS, I\dot{\Theta}), \\ I\ddot{\Theta} &= q_2(IS, I\dot{S}, I\dot{\Theta}, I\ddot{\Theta}), \end{aligned}$$

where q_1, q_2 represent the nonlinear terms of the equation. The linearised system is

$$I\ddot{S} = 2IS, \tag{4.21a}$$

$$I\ddot{\Theta} = 0, \tag{4.21b}$$

subject to the boundary and matching conditions

$$\lim_{\lambda\to\pm\infty} IS(\lambda) = 0, \; IS(0) = s_{min} - 1, \tag{4.22a}$$

$$\lim_{\lambda\to\pm\infty} I\Theta(\lambda) = 0, \tag{4.22b}$$

where $s_{min} \in [0,1]$, is the minimum value of s. We note that the second condition in (4.22a) ensures $s(0) = s_{min}$.

Using the conditions (4.22a), the general solution of (4.21a) is

$$s(y) = \begin{cases} 1 + (s_{min}-1)e^{-\sqrt{2}\frac{y}{\sqrt{L^*}}} & \text{for } 0 \le y \le 1 \\ 1 + (s_{min}-1)e^{\sqrt{2}\frac{y}{\sqrt{L^*}}} & \text{for } -1 \le y \le 0. \end{cases} \tag{4.23}$$

With IS determined, we calculate $I\Theta$. Solving (4.21b) subject to the limiting conditions (4.22b), it is clear that $I\Theta = 0$. Hence,

$$\theta(y) = \begin{cases} \frac{p_x}{(2+L_2)}\left(\frac{y^3}{6} - \frac{y}{6}\right) + \frac{k\pi}{2}(y-1) + \omega\pi & \text{for } 0 < y \leq 1 \\ \frac{p_x}{(2+L_2)}\left(\frac{y^3}{6} - \frac{y}{6}\right) + \frac{k\pi}{2}(y+1) - \omega\pi & \text{for } -1 \leq y < 0. \end{cases} \tag{4.24}$$

The expressions, (4.23) and (4.24), are consistent with our definition of an OR-type solution.

4.2. OR-type solutions for active nematodynamics, in the $L^* \to 0$ limit. Next, we consider a system of uniaxial active nematics in a channel geometry i.e., a system that is constantly driven out of equilibrium by internal stresses and activity [18]. There are three dependent variables to solve for - the concentration, c, of active particles; the fluid velocity $\mathbf{u}$, and the nematic order parameter, $\mathbf{Q}$. The corresponding evolution equations are taken from [17, 16], with additional stresses from the self-propelled motion of the active particles and the non-equilibrium intrinsic activity, referred to as *active stresses*:

$$\frac{Dc}{Dt} = \nabla \cdot \left(\mathbf{D}\nabla c + \alpha_1 c^2 (\nabla \cdot \mathbf{Q})\right), \tag{4.25a}$$

$$\nabla \cdot \mathbf{u} = 0, \quad \rho \frac{D\mathbf{u}}{Dt} = -\nabla p + \nabla \cdot (\mu(\nabla \mathbf{u} + (\nabla \mathbf{u})^T) + \tilde{\sigma}), \tag{4.25b}$$

$$\frac{D\mathbf{Q}}{Dt} = \lambda s \mathbf{W} + \zeta \mathbf{Q} - \mathbf{Q}\zeta + \frac{1}{\gamma}\mathbf{H}, \tag{4.25c}$$

where $\mathbf{W}$ is the symmetric part of the velocity gradient tensor, α_1 is an activity parameter, and λ is the nematic alignment parameter. The stress tensor, $\tilde{\sigma} = \sigma^e + \sigma^a$, is the sum of an elastic stress due to nematic elasticity

$$\sigma^e = -\lambda s \mathbf{H} + \mathbf{QH} - \mathbf{HQ}, \tag{4.26}$$

and an active stress defined by

$$\sigma^a = \alpha_2 c^2 \mathbf{Q}. \tag{4.27}$$

Here α_2 is a second activity parameter, which describes extensile (contractile) stresses exerted by the active particles when $\alpha_2 < 0$ ($\alpha_2 > 0$).

We again consider a one-dimensional static problem, with a unidirectional flow in the x direction and take $\lambda = 0$. Then the evolution equations for $\mathbf{Q}$ are the same as those considered in the passive case, hence, making it easier to adapt the calculations in section 4.1 and draw comparisons between the passive and active cases. The isotropic to nematic phase transition is driven by the concentration of active particles and as such, we take $A = \kappa(c^* - c)/2$ and $C = \kappa c$, where $c^* = \sqrt{3\pi/2L^2}$ is the critical concentration at which this transition occurs [18, 17]. As in the passive case, we work with $A < 0$ i.e. with concentrations that favour nematic ordering.

The continuity equation (4.25a), follows from the fact that the total number of active particles must remain constant [18]. This is compatible with constant concentration, c, although solutions with constant concentration do not exist for $\alpha_1 \neq 0$. As in [10], we consider the case of constant concentration c, which is not unreasonable for small values of α_1 (see (4.25a), which can admit approximately constant solutions, $c(y)$ in the $\alpha_1 \to 0$ limit), and do not consider the concentration equation, (4.25a), in this work. We nondimensionalise the system as before, but additionally scale c by L^{-1}. In terms of $\mathbf{Q}$, the evolution equations are given by

$$\frac{\partial Q_{11}}{\partial t} = u_y Q_{12} + Q_{11,yy} + \frac{1}{L^*} Q_{11}(1 - 4(Q_{11}^2 + Q_{12}^2)), \tag{4.28a}$$

$$\frac{\partial Q_{12}}{\partial t} = -u_y Q_{11} + Q_{12,yy} + \frac{1}{L^*} Q_{12}(1 - 4(Q_{11}^2 + Q_{12}^2)), \tag{4.28b}$$

$$L_1 \frac{\partial u}{\partial t} = -p_x + u_{yy} + 2L_2(Q_{11}Q_{12,yy} - Q_{12}Q_{11,yy})_y + \Gamma(Q_{12}c^2)_y, \tag{4.28c}$$

where $\Gamma = \frac{\alpha_2 \gamma}{\kappa \mu}\sqrt{-\frac{2A}{C}}$ is a measure of activity. In the steady case, and in terms of (s, θ), the system (4.28) reduces to

$$s_{yy} = 4s\theta_y^2 + \frac{s}{L^*}\left(s^2 - 1\right), \tag{4.29a}$$

$$s\theta_{yy} = \frac{1}{2} s u_y - 2 s_y \theta_y, \tag{4.29b}$$

$$u_{yy} = p_x - L_2(s^2\theta_y)_{yy} - \Gamma\left(\frac{c^2 s}{2}\sin(2\theta)\right)_y. \tag{4.29c}$$

Regarding boundary conditions, we impose the same boundary conditions on s, θ and u, as in the passive case.

The equations, (4.29a) and (4.29b), are identical to the equations, (2.5a) and (2.5b), respectively. Hence, the asymptotics in subsection 4.1 remain largely unchanged, with differences coming from (4.29c), due to the additional active stress. Substituting (4.1) into (4.29c), we obtain

$$\left(u_y + \frac{L_2}{2} s^2 u_y + \frac{\Gamma}{2} c^2 s \sin(2\theta)\right)_y = p_x. \tag{4.30}$$

Following the same steps as in subsection 4.1 to obtain equation (4.5), we compute

$$u(y) = \int_{-1}^{y} \frac{2p_x Y + 2B_0 - \Gamma c^2 s(Y)\sin(2\theta(Y))}{2g(s(Y))} dY,$$

where B_0 is a constant and g is given by (4.4). Using $u(1) = 0$ and rearranging, we see that

$$B_0 = \frac{-\int_{-1}^{1} \frac{2p_x Y - \Gamma c^2 s(Y)\sin(2\theta(Y))}{2g(s(Y))} dY}{\int_{-1}^{1} g(s(Y))^{-1} dY}.$$

From our assumption that s is even and θ is odd, it follows that $\frac{y}{g(s)}$ and $\frac{s\sin(2\theta)}{g(s)}$ are odd, and consequently, $B_0 = 0$. Therefore, the flow velocity is given by

$$u(y) = \int_{-1}^{y} \frac{2p_x Y - \Gamma c^2 s(Y)\sin(2\theta(Y))}{2g(s(Y))} dY, \tag{4.31}$$

and the velocity gradient by

$$u_y(y) = \frac{p_x y}{g(s(y))} - \frac{\Gamma c^2 s(y)\sin(2\theta(y))}{2g(s(y))}. \tag{4.32}$$

Here, the active contribution is captured by the second term, assuming a constant concentration c.

As (4.29a) and (4.29b) are identical to equations (2.5a) and (2.5b) respectively, much of the calculations are the same as in subsection 4.1. In particular, we pose asymptotic expansions as in (4.8a) and (4.8b), for s and θ respectively in the $L^* \to 0$ limit, which yields (4.9a) and (4.9b). In fact, the expression for s is given by (4.23), in the active case too. We highlight the differences for the outer solution Θ as a result of the velocity gradient (4.32). We again solve (4.13) and find an implicit representation for Θ as given below:

(4.33)
$$\Theta(y) = \begin{cases} \int_y^1 \frac{u(0)-u(Y)}{2} dY + \left(\frac{k\pi}{2} - \int_0^1 \frac{u(Y)-u(0)}{2} dY\right)(y-1) + \omega\pi, \ 0 < y \leq 1 \\ \int_{-1}^y \frac{u(Y)-u(0)}{2} dY + \left(\frac{k\pi}{2} - \int_{-1}^0 \frac{u(Y)-u(0)}{2} dY\right)(y+1) - \omega\pi, \ -1 \leq y < 0 \end{cases}$$

where $u(y)$ is given by (4.31). Moving to the inner solution $I\Theta$, we need to solve (4.21b), subject to the matching condition (4.22b). As before, we find $I\Theta = 0$, and our composite expansion for θ is just the outer solution presented above. We deduce that OR-type solutions are still possible in an active setting, for the case $\lambda = 0$.

We now consider a simple case for which (4.33) can be solved explicitly. In (4.31), we assume $s = 1$ and $\sin 2\theta = 1$ for $-1 \leq y < 0$, and $\sin(2\theta) = -1$ for $0 < y \leq 1$ i.e., we assume an OR solution with $\theta = \mp\frac{\pi}{4}$ and $\omega = -\frac{1}{4}$. Under these assumptions, integrating (4.32) yields

$$u(y) = \begin{cases} \frac{p_x}{2+L_2}(y^2-1) + \frac{\Gamma c^2}{2+L_2}(y-1), & \text{for } 0 < y \leq 1 \\ \frac{p_x}{2+L_2}(y^2-1) - \frac{\Gamma c^2}{2+L_2}(y+1), & \text{for } -1 \leq y < 0. \end{cases} \tag{4.34}$$

Substituting the above into (4.33), we find

(4.35)
$$\theta(y) = \begin{cases} \frac{p_x}{2+L_2}\left(\frac{y^3}{6} - \frac{y}{6}\right) + \frac{\Gamma c^2}{2+L_2}(\frac{y^2}{4} - \frac{y}{4}) + \frac{k\pi}{2}(y-1) + \omega\pi, & \text{for } 0 < y \leq 1, \\ \frac{p_x}{2+L_2}\left(\frac{y^3}{6} - \frac{y}{6}\right) - \frac{\Gamma c^2}{2+L_2}(\frac{y^2}{4} + \frac{y}{4}) + \frac{k\pi}{2}(y+1) - \omega\pi & \text{for } -1 \leq y < 0. \end{cases}$$

We expect (4.34) and (4.35) to be good approximations to OR-type solutions with $\omega = -\frac{1}{4}$, in the limit of small Γ (small activity) and small pressure gradient, when the outer solution is well approximated by an OR solution.

4.3. Numerical results. We solve the dynamical systems (2.4) and (4.28) with finite element methods, and all simulations are performed using the open-source package FEniCS [24]. The details of the numerical methods are given in the supplementary material. In the numerical results that follow, we extract the s profile from $\mathbf{Q}$, using (2.3). We also plot $s/2$ instead of s. We do this so that the $\mathbf{Q}$ and s-profiles fit nicely on the same axis and in our error plots, we compare (4.23)$\times 1/2$ to $s/2$. Henceforth, we will not make this distinction, and regard the plotted profiles as s.

4.3.1. Passive flows. We begin by investigating whether OR-type solutions exist for the passive system (2.4) when L^* is large (small ϵ), that is, for small nanoscale channel domains. When $\omega = \pm\frac{1}{4}$ and $p_x = -1$, we find profiles which are small perturbations of the OR solutions found in section 3, for large L^* with $p_x = 0$, i.e., the profile in (3.26) when $\omega = \pm\frac{1}{4}$ (see Fig. 3). We regard these profiles as being OR-type solutions although $s(0) \neq 0$ but $s(0) \ll 1$, as the director profile resembles a polydomain structure and θ jumps around $y = 0$, to satisfy its boundary conditions.

As $|p_x|$ increases, we lose this approximate zero in s i.e., we lose the domain wall and $s \to 1$ almost everywhere. It is also worth noting, that the director represents a splay deformation when $\omega = -\frac{1}{4}$, and a bend deformation when $\omega = \frac{1}{4}$, which becomes more pronounced as $|p_x|$ increases.

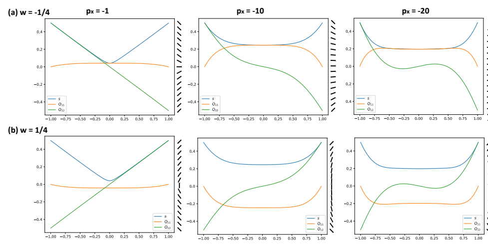

FIG. 3. *The stable solutions of* (2.4) *for* $L^* = \infty$ *(i.e., we remove the bulk contributions) and* $L_2 = 1e-3$*. The values of* p_x *and* ω*, are indicated in the plots (the same comments apply to all other figures where values are included in the plots).*

We now proceed to study solutions of (2.4) in the $L^* \to 0$ limit, relevant for micron-scale channel domains. We are interested in the stable equilibrium solutions and the existence of OR-type solutions in this limit, and how well the OR-type solutions are approximated by the asymptotic expansions in Section 4.1. As expected, in Fig. 4 we find stable equilibria which satisfy $s = 1$ almost everywhere. We also report unstable OR-type solutions in Fig. 5, when $\omega = -\frac{1}{4}$. We again consider these to be OR-type solutions despite $s(0) \neq 0$, since their behaviour is consistent with the asymptotic expressions (4.23) and (4.24), and we also have approximate polydomain structures. We also find these OR-type solutions for $\omega = \frac{1}{4}$, but do not report them as they are similar to the $\omega = -\frac{1}{4}$ case (the same is true in the next subsection). In fact, $\omega = \pm\frac{1}{4}$ are the only boundary conditions for which we have been able to identify OR-type solutions (identical comments apply to the active case).

In Fig. 5, we present three distinct OR-type solutions which vary in their Q_{11} and Q_{12} profiles, or equivalently the rotation of θ between the bounding plates at $y = \pm 1$. These numerical solutions are found by taking (4.23) (with $s_{min} = 0$) and (4.24) with different values of k ($k = 0, 1, 2$), as the initial condition in our Newton solver. We conjecture that one could build a hierarchy of OR-type solutions corresponding to arbitrary integer values of k in (4.17), or different jumps in θ at $y = 0$ in (4.17), when $\omega = \pm\frac{1}{4}$. OR-type solutions are unstable, and we speculate that the solutions corresponding to different values of k in (4.17) are unstable equilibria with different Morse indices, where the Morse index is a measure of the instability of an equilibrium point [22]. A higher value of k could correspond to a higher Morse index or informally speaking, a more unstable equilibrium point with more directions of instability. A further relevant observation is that according to the asymptotic expansion (4.24), $Q_{11}(0\pm) = 0$ and $Q_{12}(0\pm) = \pm\frac{1}{2}$, and hence the energy of the domain wall does not depend strongly on k. The far-field behavior does depend on k in (4.24), and we conjecture that this k-dependence generates the family of k-dependent OR-type equilibrium solutions. We note that OR-type solutions generally do not satisfy $s(0) = 0$, but typically exhibit polydomain structures in θ, or equivalently the director $\mathbf{n} = (\cos\theta, \sin\theta)$. However, as L^* decreases, we find $s(0) \to 0$ for OR-type solutions, for a fixed p_x (see Fig. 6).

To conclude this section on passive flows, we assess the accuracy of our asymptotic expansions in section 4.1. In Fig. 7, we plot the error between the asymptotic

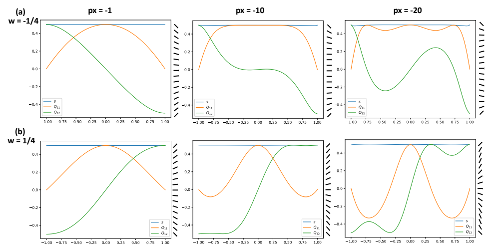

FIG. 4. *Some example stable solutions of* (2.4) *for* $L^* = 1e-3$ *and* $L_2 = 1e-3$.

expressions ((4.23) and (4.24)) and the corresponding numerical solutions of (2.4), for the parameter values $L^* = 1e-4$, $L_2 = 1e-3$, $p_x = -20$ and $\omega = -\frac{1}{4}$. More precisely, we use these parameter values along with $k = 1, 2, 3$ in (4.24), and (4.23) with $s_{min} = 0$, to construct the asymptotic profiles. We then use these asymptotic profiles as initial conditions to find the corresponding numerical solutions. Hence, we have three comparison plots in Fig. 7, corresponding to $k = 1, 2, 3$ respectively. By error, we refer to the difference between the asymptotic profile and the corresponding numerical solution. We label the asymptotic profiles using the superscript 0, in the $L^* \to 0$ limit, whilst a nonzero superscript identifies the numerical solution along with the the value of L^* used in the numerics (these comments also apply to the active case in the next section). We find good agreement between the asymptotics and numerics, especially for the s profiles, where any error is confined to a narrow interval around $y = 0$ and does not exceed 0.07 in magnitude. Using (2.2), (4.23), and (4.24), we construct the corresponding asymptotic profile $\mathbf{Q}^0$. Looking at the differences between $\mathbf{Q}^0$ and the numerical solutions $\mathbf{Q}^{1e-4}$ (for $k = 1, 2, 3$), the error does not exceed 0.06 in magnitude. This implies good agreement between the asymptotic and numerically computed θ-profiles, at least for the parameter values under consideration. While the fluid velocity u is not the focus of this work, we note that our asymptotic profile (4.14), gives almost perfect agreement with the numerical solution for u.

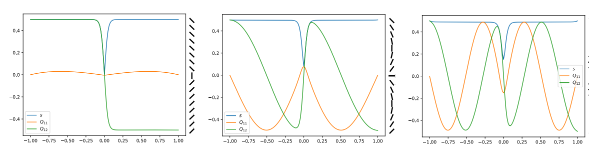

FIG. 5. *Three unstable OR-type solutions of* (2.4) *for* $L^* = 1e-3$, $L_2 = 1e-3$, $p_x = -1$ *and* $\omega = -\frac{1}{4}$. *The initial conditions used are* (4.23) *(with* $s_{min} = 0$*) and* (4.24) *with* $k = 0, 1, 2$ *(from left to right), along with the parameter values just stated.*

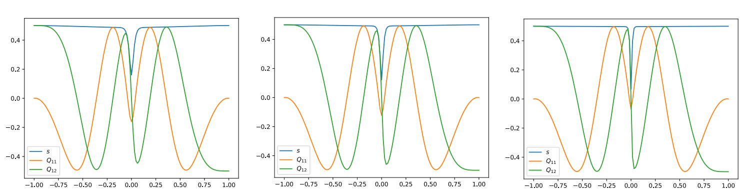

FIG. 6. *Plot of an OR-type solution for* $L^* = 5e-4$, $3e-4$, $1e-4$ *(from left to right). The remaining parameter values are* $L_2 = 1e-3$, $p_x = -20$ *and* $\omega = -\frac{1}{4}$. *The initial conditions used are* (4.23) *(with* $s_{min} = 0$*) and* (4.24) *with* $k = 2$, *along with the parameter values just stated.*

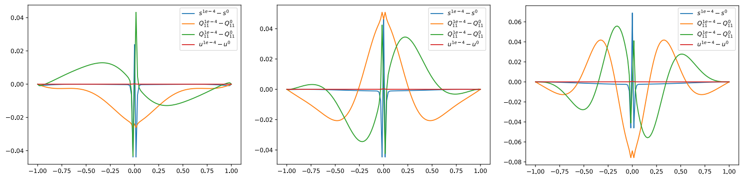

FIG. 7. *Plot of* $\mathbf{Q}^{1e-4} - \mathbf{Q}^0$*,* $s^{1e-4} - s^0$*, and* $u^{1e-4} - u^0$*. Here,* $\mathbf{Q}^0$ *is the asymptotic profile given by* (4.23) *and* (4.24) *with,* $s_{min} = 0$*,* $k = 1, 2, 3$ *(from left to right),* $L^* = 1e-4$*,* $L_2 = 1e-3$*,* $p_x = -20$ *and* $\omega = -1/4$*, whilst* $\mathbf{Q}^{1e-4}$ *denotes the corresponding numerical solution of* (2.4)*.* s^0 *is given by* (4.23) *and* s^{1e-4} *is extracted from* $\mathbf{Q}^{1e-4}$*. The numerical solutions are found by using* $\mathbf{Q}^0$ *as the initial condition. Identical comments apply to* $u^0 - u^{1e-4}$*, where* u^0 *is given by* (4.14) *and* u^{1e-4} *is the numerical solution of* (2.4)*.*

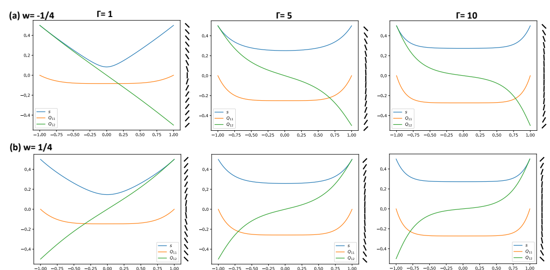

FIG. 8. *The stable solutions of* (4.28) *for* $L^* = \infty$ *,* $L_2 = 1e-3$*,* $c = \sqrt{2\pi}$ *and* $p_x = -1$*.*

4.3.2. Active flows. As explained previously, we consider active flows with constant concentration c, and take $c > c^*$. To this end, we fix $c = \sqrt{2\pi}$ in the following numerical experiments. For L^* large (small nano-scale channel domains), we find OR-type solutions when $\omega = \pm\frac{1}{4}$, and these are stable. In Fig. 8, we plot these solutions when $p_x = -1$ and for three different values of Γ, which we recall is proportional to the activity parameter α_2. We only have $s(0) \approx 0$ when $\Gamma = 1$, in which case the director profile exhibits polydomain structures. As Γ increases, $s(0)$ increases and $s \to 1$ almost everywhere, so that OR-type solutions are only possible for small values of p_x and Γ. Increasing $|p_x|$ for a fixed value of Γ, also drives $s \to 1$ everywhere. Looking at Fig. 3 and 8 together, we notice that if Q_{11} is positive in the interior, the nematic director has a splay deformation and if Q_{11} is negative in the interior, the director has a bend deformation.

As in the passive case, we also find unstable OR-type solutions consistent with the limiting asymptotic expression (4.23), along with a discontinuous θ profile as in (4.33), for small values of L^* that correspond to micron-scale channels. The stable solutions have $s \approx 1$ almost everywhere (see Fig. 9). In Fig. 10, we find unstable OR-type solutions when $L^* = 1e-3$, $L_2 = 1e-3$ and $\omega = -\frac{1}{4}$, for a range of values of p_x and Γ. To numerically compute these solutions, we use the stated parameter values in (4.23) (with $s_{min} = 0$) and (4.35), along with $k = 0$, as our initial condition. We only have $s(0) \approx 0$ provided $|p_x|$ and Γ are not too large, however, $s(0) \to 0$ in the $L^* \to 0$ limit for fixed values of p_x and Γ. This illustrates the robustness of OR-type solutions in an active setting. In Fig. 11, we plot three further distinct OR-type solutions, obtained by taking (4.23) (with $s_{min} = 0$) and (4.35) with $k = 1, 2, 3$, as our initial condition. Hence, for the same reasons as in the passive case, we believe there may be multiple unstable OR-type solutions, corresponding to different values of k in (4.17).

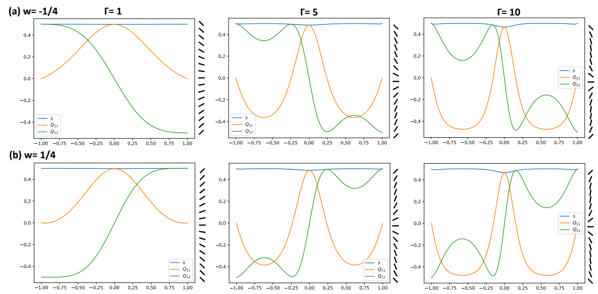

FIG. 9. *The stable solutions of* (4.28) *for* $L^* = 1e-3$, $L_2 = 1e-3$, $c = \sqrt{2\pi}$ *and* $p_x = -1$.

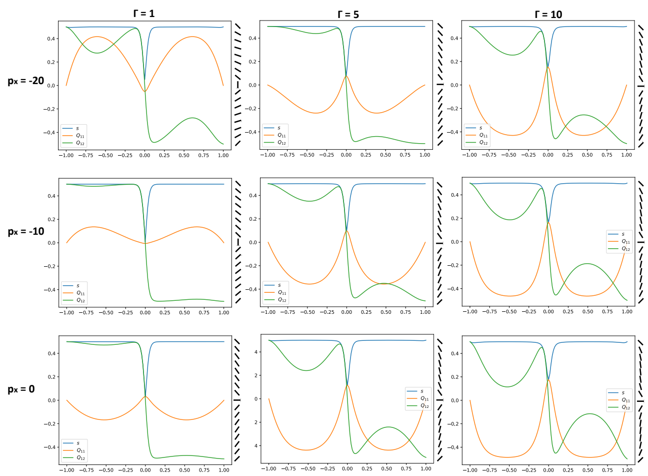

FIG. 10. *Unstable OR-type solutions of* (4.28), *for* $L^* = 1e-3$, $L_2 = 1e-3$, $c = \sqrt{2\pi}$ *and* $\omega = -\frac{1}{4}$. *The initial conditions used are* (4.23) *(with* $s_{min} = 0$*) and* (4.35) *with* $k = 0$.

By analogy with the passive case, we now compare the asymptotic expressions (4.23), (4.34) and (4.35), with the numerical solutions. The error plots are given in Fig. 12. Once again, there is good agreement between the limiting s-profile (4.23) and the numerical solutions, where any error is confined to a small interval around $y = 0$. There is also good agreement between the asymptotic and numerically computed θ-profiles (coded in terms of Q_{11} and Q_{12}) and flow profile u, provided $|p_x|$, Γ, or both, are not too large. When $|p_x|$ and Γ are large (say much greater than 1), the accuracy of the asymptotics breaks down, especially for the u-profile. However, OR-type solutions are still possible for large values of $|p_x|$ and Γ, as elucidated by Fig. 10.

5. Conclusions. In this article, we have demonstrated the universality of OR-type solutions in NLC-filled microfluidic channels. Section 3 focuses on the simple and idealised case of constant flow and pressure to give some preliminary insight into the more complex systems considered in section 4. We prove a series of results that lead to the interesting and non-obvious conclusion, that the multiplicity of observable equilibria depend on the boundary conditions. We employ a (s, θ)-formalism for the NLC state, and impose Dirichlet conditions for (s, θ) coded in terms of ω, where ω is a measure of the director rotation between the bounding plates $y = \pm 1$. We always have a unique smooth solution in this framework provided an OR solution does not

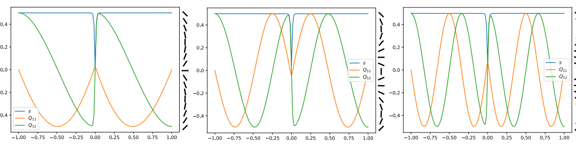

FIG. 11. *Three unstable OR-type solutions of* (4.28) *for* $L^* = 1e-3$*,* $L_2 = 1e-3$*,* $p_x = -1$*,* $\Gamma = 0.7$ *and* $\omega = -\frac{1}{4}$*.*

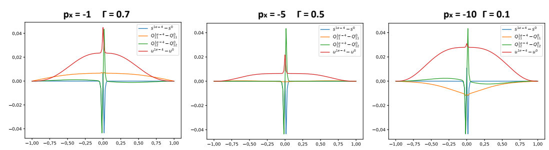

FIG. 12. *Plot of* $\mathbf{Q}^{1e-4} - \mathbf{Q}^0$*,* $s^{1e-4} - s^0$*, and* $u^{1e-4} - u^0$*. Here,* $\mathbf{Q}^0$ *is given by* (4.23) *and* (4.35) *with,* $s_{min} = 0$*,* $k = 0$*,* $c = \sqrt{2\pi}$*,* $L^* = 1e-4$*,* $L_2 = 1e-3$*,* p_x *and* Γ *as stated in the figure, and* $\omega = -1/4$*, whilst* $\mathbf{Q}^{1e-4}$ *is the numerical solution of* (4.28)*, with the same parameter values.*

exist (Theorem 3.4). Additionally, in the $\mathbf{Q}$-framework for $\omega = \pm\frac{1}{4}$ i.e., when the boundary conditions are orthogonal to each other, OR solutions with polydomain structures exist for all values of L^* or ϵ, they are globally stable for large L^* (small ϵ), and there are multiple solutions for small values of L^* (large ϵ) or large channel geometries. In fact, for all three scenarios considered in this paper, we have found OR and OR-type solutions to be compatible with $\omega = \pm\frac{1}{4}$ only, or orthogonal boundary conditions. We note that in Theorem 7 of [3], the author proves that minimizers of an Oseen-Frank energy in three dimensions are unique for non-orthogonal boundary conditions. This result is clearly different from ours, based on different arguments, but has a similar physical flavour. As has been noted in [2] amongst others, orthogonal boundary conditions allow for solutions in the $\mathbf{Q}$-formalism (solutions of (3.1)) that have a constant set of eigenvectors in space. These solutions, with a constant set of eigenvectors, are precisely the OR solutions, which are disallowed for non-orthogonal boundary conditions. Thus, whilst the conclusion of Theorem 3.1 is not surprising on physical grounds, or by comparison with previous work for other continuum NLC models, we recover the same result with a different set of arguments in the (s,θ)-framework, which is of independent interest.

In section 4, we calculate useful asymptotic expansions for OR-type solutions in the limit of large domains, for both passive and active nematics. The asymptotics are validated by numerically computed OR-type solutions for small and large values of L^*, using the asymptotic expansions as initial conditions. There is good agreement between the asymptotics and the numerical solutions, and the asymptotics give good insight into the internal structure of domain walls of OR-type solutions and the outer far-field solutions. These techniques can be further embellished to include external fields, other types of boundary conditions and more complex geometries too.

In section 4.3, the OR-type solutions are unstable for small L^* or large channels. However, they may still be observable and hence, physically relevant. Referring to the experimental results in [1] for passive NLC-filled microfluidic channels, the authors find disclination lines at the centre of a microfluidic channel filled with the liquid crystal 5CB, with flow, and with and without an applied electric field. Moreover, the authors are able to stabilise these disinclination lines by applying an electric field. So, while the OR-type solutions are unstable mathematically, they can be stabilised or controlled/exploited for transport phenomena and cargo transport in experiments. In the active case, there are similar experimental results in [20]. Here the authors use an applied magnetic field to control an active nematic system (8CB with a water based active gel), and find lanes of defect cores running parallel to the channel walls. These defect cores and disclination lines can be modelled by OR-type solutions, as we have studied in this paper. In general, we argue that unstable solutions are of independent interest since they play crucial roles in the connectivity of solution landscapes of complex systems [22]. Unstable solutions steer the dynamics of a system and ultimately, dictate the selection of the steady state for multistable systems (with multiple stable states). Hence, OR-type solutions are unstable for large domains, but can influence non-equilibrium properties and can be stabilised for tailor-made applications.

To conclude this article, we argue why OR-type solutions maybe universal in variational theories, with free energies that employ a Dirichlet elastic energy for the unknowns, e.g. $y_1 \dots y_n$ for $n \in \mathbb{N}$. Working in a one-dimensional setting, consider an energy of the form

$$\int_\Omega y_1'(x)^2 + \dots y_n'(x)^2 + \frac{1}{L^*} h(y_1, \dots y_n)(x) \, \mathrm{d}x, \tag{5.1}$$

subject to Dirichlet boundary conditions, for a material-dependent positive elastic constant L^*. The function, h, models a bulk energy that only depends on $y_1, \dots, y_n$. As $L^* \to \infty$, the limiting Euler-Lagrange equations admit unique solutions of the form $y_j = ax + b$, for constants a and b. For specific choices of Ω and asymmetric boundary conditions, we can have domain walls at $x = x^*$ such that $y_j(x^*) = 0$ for $j = 1, \dots, n$. Writing each $y_j = |y_j| sgn(y_j)$, the domain wall separates polydomains with phases differentiated by different values of $sgn(y_j)$. Moreover, we believe this argument can be extended to systems in two and three-dimensions.

Acknowledgments. We thank Giacomo Canevari for helpful comments on some of the proofs in Section 3.

Taxonomy. The author names are listed alphabetically. JD led the project, which was conceived and designed by AM and LM. YH produced all the numerics and contributed to the analysis. JD, AM and LM wrote the manuscript carefully and oversaw the project evolution. AM mentored JD and YH throughout the project.

REFERENCES

[1] H. Agha and C. Bahr, *Nematic line defects in microfluidic channels: wedge, twist and zigzag disclinations*, Soft Matter, 14 (2018), pp. 653–664.

[2] L. Ambrosio and E. G. Virga, *A boundary-value problem for nematic liquid crystals with a variable degree of orientation*, Arch. Ration. Mech. Anal., 114 (1991), pp. 335–347.

[3] J. Ball, *Mathematics and liquid crystals*, Molecular Crystals and Liquid Crystals, 647 (2017), pp. 1–27.

[4] A. N. Beris and B. J. Edwards, *Thermodynamics of Flowing Systems: With Internal Microstructure*, Oxford University Press, Oxford, UK, 1994.

[5] F. Bethuel, H. Brezis, and F. Hélein, *Asymptotics for the minimization of a Ginzburg–Landau functional*, Calc. Var. Partial Diff., 1 (1993), pp. 123–148.

[6] A. Braides, *A handbook of Γ-convergence*, in Handbook of Differential Equations: Stationary Partial Differential Equations, vol. 3, Elsevier, North-Holland, Amsterdam, 2006, pp. 101–213.

[7] M. Calderer and B. Mukherjee, *Chevron patterns in liquid crystal flows*, Physica D: Nonlinear Phenomena, 98 (1996), p. 201–224.

[8] G. Canevari, J. Harris, A. Majumdar, and Y. Wang, *The well order reconstruction solution for three-dimensional wells, in the Landau–de Gennes theory*, Int. J. Nonlin. Mech., 119 (2020), p. 103342.
[9] G. Canevari, A. Majumdar, and A. Spicer, *Order reconstruction for nematics on squares and hexagons: a Landau–de Gennes study*, SIAM J. Appl. Math., 77 (2019), pp. 267–293.
[10] G.-Q. Chen, A. Majumdar, D. Wang, and R. Zhang, *Global existence and regularity of solutions for active liquid crystals*, J. Differential Equations, 263 (2017), pp. 202–239.
[11] S. Čopar, Ž. Kos, T. Emeršič, and U. Tkalec, *Microfluidic control over topological states in channel-confined nematic flows*, Nature communications, 11 (2020), pp. 1–10.
[12] J. Cuennet, A. E. Vasdekis, and D. Psaltis, *Optofluidic-tunable color filters and spectroscopy based on liquid-crystal microflows*, Lab on a Chip, 13 (2013), pp. 2721–2726.
[13] J. Dalby, P. Farrell, A. Majumdar, and J. Xia, *One-dimensional ferronematics in a channel: order reconstruction, bifurcations and multistability*, SIAM J. Appl. Math. accepted, (2021).
[14] P. G. de Gennes, *The Physics of Liquid Crystals*, Oxford University Press, Oxford, 1974.
[15] L. Fang, A. Majumdar, and L. Zhang, *Surface, size and topological effects for some nematic equilibria on rectangular domains*, Math. Mech. Solids, 25 (2020), pp. 1101–1123.
[16] L. Giomi, M. Bowick, X. Ma, and M. Marchetti, *Defect annihilation and proliferation in active nematics*, Phys. Rev. L, 110 (2013), pp. 228101–1–228101–5.
[17] L. Giomi, M. Bowick, P. Mishra, R. Sknepnek, and M. Marchetti, *Defect dynamics in active nematics*, Phil. Trans. R.Soc. A, 372 (2014), p. 20130365.
[18] L. Giomi, L. Mahadevan, B. Chakraborty, and M. Hagan, *Banding, excitability and chaos in active nematic suspensions*, Nonlinearity, 25 (2012), p. 2245–2269.
[19] D. Golovaty, J. Montero, and P. Sternberg, *Dimension Reduction for the Landau-de Gennes Model in Planar Nematic Thin Films*, J. Nonlinear Sci, 25 (2015), pp. 1431–1451.
[20] P. Guillamat, J. Ignés-Mullol, and F. Sagués, *Control of active liquid crystals with a magnetic field*, Proceedings of the National Academy of Sciences, 113 (2016), pp. 5498–5502.
[21] Y. Han, A. Majumdar, and L. Zhang, *A reduced study for nematic equilibria on two-dimensional polygons*, SIAM J. Appl. Math, 80 (2020), pp. 1678–1703.
[22] Y. Han, J. Yin, P. Zhang, A. Majumdar, and L. Zhang, *Solution landscape of a reduced landau-de gennes model on a hexagon*, Nonlinearity, 34 (2021), pp. 2048–2069.
[23] X. Lamy, *Bifurcation analysis in a frustrated nematic cell*, J. Nonlinear Sci., 24 (2014), pp. 1197–1230.
[24] A. Logg, K.-A. Mardal, and G. Wells, *Automated solution of differential equations by the finite element method: The FEniCS book*, vol. 84, Springer Science & Business Media, 2012.
[25] J. E. Maclennan, M. A. Handschy, and N. A. Clark, *Director reorientation dynamics in chevron ferroelectric liquid crystal cells*, Liquid Crystals, 7 (1990), pp. 787–796.
[26] A. Majumdar, *Equilibrium order parameters of nematic liquid crystals in the Landau–de Gennes theory*, Euro. J. Appl. Math, 21 (2010), pp. 181–203.
[27] M. C. Marchetti, J.-F. Joanny, S. Ramaswamy, T. B. Liverpool, J. Prost, M. Rao, and R. A. Simha, *Hydrodynamics of soft active matter*, Reviews of Modern Physics, 85 (2013), p. 1143.
[28] S. Mondal, I. Griffiths, F. Charlet, and A. Majumdar, *Flow and nematic director profiles in a microfluidic channel: the interplay of nematic material constants and backflow*, Fluids, 3 (2018), p. 39.
[29] L. Mrad and D. Phillips, *Dynamic analysis of chevron structures in liquid crystal cells*, Molecular Crystals and Liquid Crystals, 647 (2017), pp. 66–91.
[30] T. P. Rieker, N. A. Clark, G. S. Smith, D. S. Parmar, E. B. Sirota, and C. R. Safinya, *"chevron" local layer structure in surface-stabilized ferroelectric smectic-c cells*, Phys. Rev. Lett., 59 (1987), pp. 2658–2661.
[31] A. Sengupta, C. Bahr, and S. Herminghaus, *Topological microfluidics for flexible micro-cargo concepts*, Soft Matter, 9 (2013), pp. 7251–7260.
[32] Y. Wang, G. Canevari, and A. Majumdar, *Order reconstruction for nematics on squares with isotropic inclusions: a Landau–de Gennes study*, SIAM J. Appl. Math., 79 (2019), pp. 1314–1340.

Supplementary materials. A Multi-Faceted Study of Nematic Order Reconstruction in Microfluidic Channels.

1. Supplementary material for section 3 - Passive flows with constant velocity and pressure. Here we present supplementary material for section 3 of the main text. Any references to equations and Theorems not appearing in this document, refer to equations and Theorems in the main text.

THEOREM 1.1. *(Maximum Principle) Let s and θ be solutions of* (3.3a) *and* (3.3b)*, where s is at least C^1, then*

$$0 < s \leq 1 \quad \forall y \in [-1,1]. \tag{1.1}$$

Proof. Let (s,θ) denote a solution pair of (3.3a) and (3.3b), and assume for contradiction that s has a local minimum at $\hat{y}$, such that $s(\hat{y}) \leq 0$. This implies that $B = 0$ using (3.3b). If $B = 0$, then we must have either $s = 0$ everywhere or a piecewise constant θ-profile. The first case is inadmissible and the second case is simply an OR solution, determined by the ordinary differential equation:

$$s'' = \epsilon s(s^2 - 1), \tag{1.2}$$

which can be integrated to obtain the scalar order parameter. Doing this, we find

$$s' = \pm\sqrt{\left(\epsilon\left(\frac{s^4}{2} - s^2\right) + A\right)}. \tag{1.3}$$

Evaluating at $s = 1$, we see $A \geq \frac{\epsilon}{2}$. At the minimum, $s'(\hat{y}) = 0$, hence

$$s^2(\hat{y}) = 1 \pm \sqrt{1 - \frac{2A}{\epsilon}}, \tag{1.4}$$

which requires $A \leq \frac{\epsilon}{2}$. Combining these inequalities yields $A = \frac{\epsilon}{2}$. We then have

$$s' = \pm\sqrt{\frac{\epsilon}{2}(s^2-1)^2}.$$

Fixing the sign in the above to be either positive or negative, we have a first order ODE subject to the boundary condition $s(-1) = 1$, or $s(1) = 1$. In any case, $s \equiv 1$ is a solution, hence, by the Picard-Lindelöf Theorem, this is the unique solution and this is clearly positive everywhere.

We prove that $s \leq 1$ by a direct application of the maximum principle. Assume that there exists a point $y^* \in [-1,1]$ where s attains its maximum, and $s(y^*) > 1$ so that $y^* \in (-1,1)$. The function s^2 must also attain its maximum at the point $y^* \in (-1,1)$, so that

$$\left(s^2\right)''(y^*) \leq 0.$$

Next, note that $\left(s^2\right)'' = 2(s')^2 + 2ss''$. We now multiply (3.3a) by s, and substitute for $s''s$ in the resulting expression to obtain

$$\frac{1}{2}\left(s^2\right)'' = (s')^2 + 4s^2(\theta')^2 + \epsilon s^2(s^2 - 1). \tag{1.5}$$

Using $s(y^*) > 1$, (1.5) implies that $\left(s^2\right)''(y^*) > 0$, which is a contradiction. Hence, we conclude that $s \leq 1$ $\forall y \in [-1,1]$. ∎

1.1. The $\epsilon \to 0$ and $\epsilon \to \infty$ limits.

PROPOSITION 1.2. *For $\omega \neq \pm\frac{1}{4}$, $s_{0,\omega}$ has exactly one critical point at $y = 0$, which is a non-trivial global minimum i.e. $s_{0,\omega}(0) > 0$. For $\omega = \pm\frac{1}{4}$, s has exactly one minimum at $y = 0$ such that $s_{0,\pm\frac{1}{4}}(0) = 0$.*

Proof. It is clear from (3.26a) that $s_{0,\omega}(-y) = s_{0,\omega}(y)$ and as such $s_{0,\omega}$ is symmetric. We quickly note from (3.26a), that $s = 1$ when $\omega = 0, \pm\frac{1}{2}$. Next, we consider the cases $\omega \neq 0,\ \pm\frac{1}{4},\ \pm\frac{1}{2}$. Differentiating (3.26a), we have

$$s'_{0,\omega}(y) = \pm\frac{y\sin^2(2\omega\pi)}{\sqrt{\cos^2(2\omega\pi) + y^2\sin^2(2\omega\pi)}} = 0 \implies y = 0 \text{ since } \omega \neq 0, \pm\frac{1}{2}.$$

Hence, the solution has one critical point at $y = 0$, which is a global minimum. Since $s(0) = \cos(2\omega\pi)$, this minimum is non-trivial for $\omega \neq \pm\frac{1}{4}$.

Next, we briefly consider the case when $\omega = \pm\frac{1}{4}$. From (3.26a) we see that the solution is given by

$$s_{0,\pm\frac{1}{4}}(y) = \begin{cases} -y & \text{for } y \in [-1,0] \\ y & \text{for } y \in [0,1], \end{cases}$$

which clearly has a unique minimum value $y = 0$, and $s_{0,\pm\frac{1}{4}}(0) = 0$. We have a domain wall at $s = 0$, and $\theta_{0,\frac{1}{4}} = -\frac{\pi}{4}$ for $y < 0$ and $\theta_{0,\frac{1}{4}} = \frac{\pi}{4}$ for $y > 0$. Analogous remarks apply to $\omega = -\frac{1}{4}$. In other words, there are polydomain structures with distinct nematic directors, separated by a domain wall i.e. the unique limiting profile is an OR solution, and hence globally stable in the $\epsilon \to 0$ limit, for $\omega = \pm\frac{1}{4}$. ∎

OR solutions are unstable in the $\epsilon \to \infty$ limit, for $\omega = \pm\frac{1}{4}$ [23]. However, we can deduce the asymptotic profiles of OR solutions in this limit, since OR solutions exist for all ϵ, when $\omega = \pm\frac{1}{4}$. To this end, we introduce the OR energy for $\omega = \pm\frac{1}{4}$ and $Q_{11}(y) \equiv 0$ for all $y \in [-1, 1]$:

$$E(Q_{12}) := \int_{-1}^{1} (Q'_{12})^2 + \epsilon Q_{12}^2(2Q_{12}^2 - 1),\ \mathrm{d}y, \tag{1.6}$$

subject to the boundary conditions in (2.7). As $\epsilon \to \infty$, the minimizers of the OR energy converge to the set $\mathcal{B}^{OR}$ where

$$\mathcal{B}^{OR} = \left\{(Q_{11}, Q_{12}) = \left(0, \pm\frac{1}{2}\right)\right\}.$$

Focusing on $\omega = \frac{1}{4}$ and replicating arguments from [13], we deduce that OR solutions, interpreted as minimizers of (1.6), converge in $L^1([-1, 1])$, almost everywhere to a map of the form

$$\mathbf{Q}^* = \left(0, -\frac{1}{2}\right)\chi_{E_1} + \left(0, \frac{1}{2}\right)\chi_{E_2}, \tag{1.7}$$

where χ is the characteristic function of an interval, $E_1 = [-1, 0)$ and $E_2 = (0, 1]$, in the $\epsilon \to \infty$ limit.

1.2. Numerical results. We solve the time-dependent equations (2.4) with constant u, using gradient flow methods in Matlab. We use finite difference methods in the spatial direction, with a step size of $1/50$, and Euler's method in the time direction. The solution is deemed to have converged when the norm of the gradient has fallen below 10^{-6}.

In Fig. 13, we fix $\omega = \frac{1}{4}$ and $\epsilon = 10$, and demonstrate multiple solutions for different initial conditions. The black curves label the OR solution, since $s = 0$ at $y = 0$, and θ is discontinuous at $y = 0$. The red curves label smooth solutions with no domain walls. However, for $\epsilon \leq 3$ (approximately) we only observe the OR solution. In Fig. 14, we plot the (s, θ) profiles for $\omega = \frac{1}{8}$, and for three different values of ϵ. Using different initial conditions, we only find one solution profile for each value of ϵ, consistent with Theorems 3.1 and 3.4. Finally, in Fig. 15, we take $\epsilon = 100$ and see if OR solutions do indeed converge to the limiting profile in (1.7), and the numerics are indeed consistent with an almost piecewise constant profile for Q_{12}, except for a transition layer localised around $y = 0$.

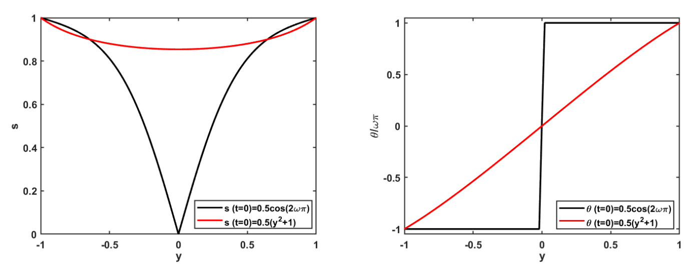

(a) (b)

FIG. 13. *Different types of (s, θ) profiles obtained by using different initial conditions. The black curves are found by taking $Q_{11} = \frac{1}{2}\cos(2\omega\pi)$ and $Q_{12} = \frac{1}{2}\sin(2\omega\pi)y$ as the initial condition, whilst the red curves are found by taking $Q_{11} = \frac{1}{2}(y^2 + 1)$ and $Q_{12} = \frac{1}{2}\sin(2\omega\pi)y$ as the initial condition. The parameter values are $\omega = \frac{1}{4}$ and $\epsilon = 10$.*

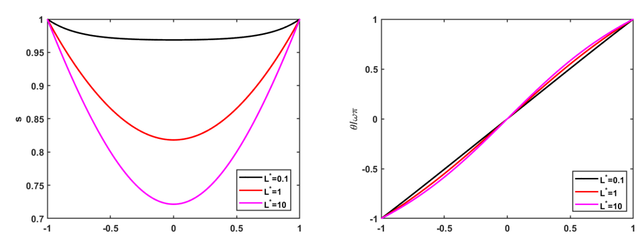

FIG. 14. *(s, θ) profiles obtained for different values of ϵ. For these values of ϵ, the initial conditions $Q_{11} = \frac{1}{2}\cos(2\omega\pi)$ and $Q_{12} = \frac{1}{2}\sin(2\omega\pi)y$, and $Q_{11} = \frac{1}{2}(y^2+1)$ and $Q_{12} = \frac{1}{2}\sin(2\omega\pi)y$, converge to the same solution. The parameter values are $\omega = \frac{1}{8}$ and $\epsilon := \frac{1}{L^*}$ as indicated in the plot.*

2. Numerical methods. Here we explain the numerical methods used in section 4.3 of the main text. We write the dynamical systems in their weak formulation. For example, the weak formulation of the complicated active system (4.28), is the

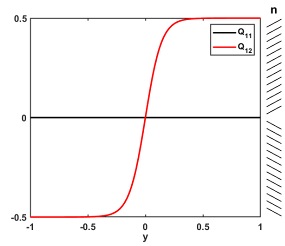

FIG. 15. *The only OR solution for $\omega = \frac{1}{4}$ and $\epsilon = 100$. The corresponding director profile is plotted on the right.*

following:

(2.1a)
$$\int_{-1}^{1} \frac{\partial Q_{11}}{\partial t} v_1 dy = \int_{-1}^{1} u_y Q_{12} v_1 - Q_{11,y} v_{1y} + \frac{1}{L^*} Q_{11}(1 - 4(Q_{11}^2 + Q_{12}^2)) v_1 \text{ d}y,$$

(2.1b)
$$\int_{-1}^{1} \frac{\partial Q_{12}}{\partial t} v_2 dy = \int_{-1}^{1} -u_y Q_{11} v_2 - Q_{12,y} v_{2y} + \frac{1}{L^*} Q_{12}(1 - 4(Q_{11}^2 + Q_{12}^2)) v_2 \text{ d}y,$$

(2.1c)
$$\int_{-1}^{1} \frac{\partial u}{\partial t} v_3 dy = \int_{-1}^{1} -p_x v_3 - \left(u_y + 2L_2(Q_{11}Q_{12,yy} - Q_{12}Q_{11,yy}) + \Gamma(Q_{12}c^2)\right) v_{3y} \text{ d}y,$$

for all $v_1, v_2, v_3 \in W_0^{1,2}([-1, 1])$ with Dirichlet boundary conditions for (Q_{11}, Q_{12}) and u, given in (2.7) and (2.8), respectively. We partition the domain $[-1, 1]$ into a uniform mesh with mesh size $h = 1/256$. Due to the third order partial derivatives with respect to y in (4.28), Lagrange elements of order 2 are used for the spatial discretization.

We also study the linear stability of the equilibrium solutions in (2.4) and (4.28). The systems can be written as $\frac{\partial \mathbf{x}}{\partial t} = F(\mathbf{x}(t))$. Let $\mathbf{x}_0$ denote an equilibrium point i.e. $F(\mathbf{x}_0) = \mathbf{0}$, and let $J(\mathbf{x}_0) = \nabla F(\mathbf{x}_0)$ be the Jacobian matrix of F at $\mathbf{x}_0$. We can then determine the stability of $\mathbf{x}_0$ by checking the sign of the largest real part amongst all eigenvalues of $J(\mathbf{x}_0)$. If the largest real part is negative (positive), then the equilibrium point is stable (unstable).

For stable states of the system (2.4), we use the semi-implicit Euler method for time discretization and the initial conditions

$$Q_{11} = \cos(2\omega\pi y)/2, \ Q_{12} = \sin(2\omega\pi y)/2, \ u = -p_x(1 - y^2)/2. \tag{2.2}$$

For the unstable OR-type solutions, we assume that the partial derivatives with respect to t are zero, and solve the passive or active flow systems using a Newton solver with a linear LU solver at each iteration. Newton's method strongly depends on the initial condition, so we use the asymptotic expressions (4.23) and (4.24) as initial conditions for the passive flow system, and (4.23) and (4.35) as initial conditions for the active flow system with small Γ. In the active case, we perform an increasing Γ sweep for the OR branch to obtain OR-type solutions for large Γ.